Cell Reports
Medicine

Article

CD103$^+$CD8$^+$ T_{RM} Cells Accumulate in Tumors of Anti-PD-1-Responder Lung Cancer Patients and Are Tumor-Reactive Lymphocytes Enriched with Tc17

Graphical Abstract

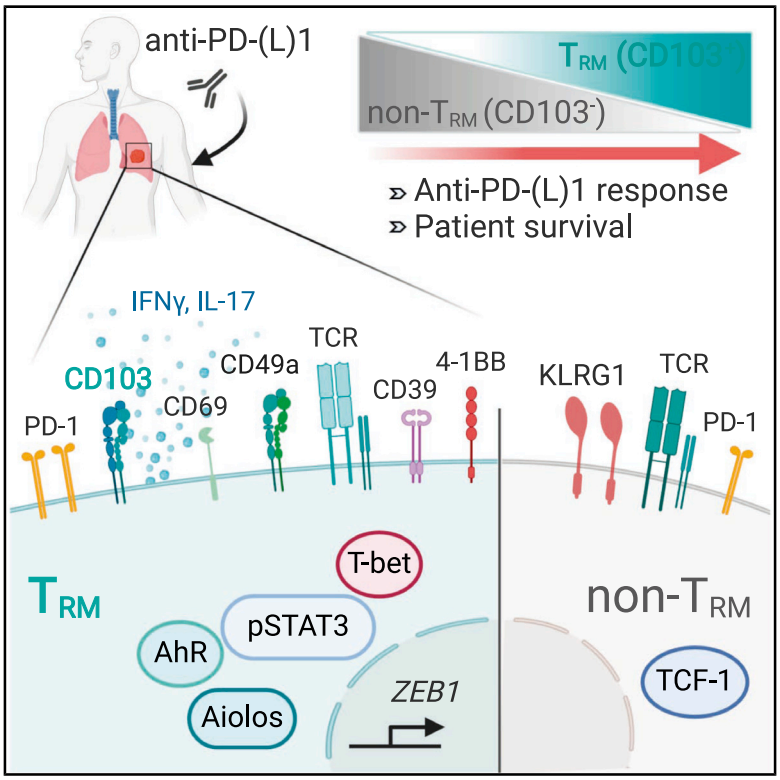

Highlights

- A high density of CD103$^+$CD8$^+$ cells in tumors correlates with response to anti-PD-(L)1
- The density of CD103$^+$CD8$^+$ cells increases after anti-PD-1 in most responder patients
- CD103$^+$CD8$^+$ T_{RM} cells are enriched with tumor-specific T cells
- A subset of CD103$^+$CD8$^+$ T_{RM} cells display a Tc17 differentiation program

Authors

Stéphanie Corgnac, Ines Malenica, Laura Mezquita, ..., Julien Adam, Benjamin Besse, Fathia Mami-Chouaib

Correspondence

fathia.mami-chouaib@gustaveroussy.fr

In Brief

Using retrospective cohorts of anti-PD-(L)1-treated NSCLC, Corgnac et al. show that the density of CD103$^+$CD8$^+$ cells in tumors is associated with better progression-free survival. CD103$^+$CD8$^+$ tumor-infiltrating lymphocytes are tumor-specific resident memory T cells (T_{RM}) enriched with a subset displaying a unique Tc1/Tc17 differentiation program that differs from CD103$^-$CD8$^+$ T cells (non-T_{RM}).

Corgnac et al., 2020, Cell Reports Medicine *1*, 100127
October 20, 2020
https://doi.org/10.1016/j.xcrm.2020.100127

CellPress

Cell Reports Medicine

CellPress
OPEN ACCESS

Article

CD103$^+$CD8$^+$ T_{RM} Cells Accumulate in Tumors of Anti-PD-1-Responder Lung Cancer Patients and Are Tumor-Reactive Lymphocytes Enriched with Tc17

Stéphanie Corgnac,[1] Ines Malenica,[1] Laura Mezquita,[2,9,10] Edouard Auclin,[3,9] Elodie Voilin,[1] Jamila Kacher,[1] Heloise Halse,[1] Laetitia Grynszpan,[1] Nicolas Signolle,[4] Thibault Dayris,[5] Marine Leclerc,[1] Nathalie Droin,[5] Vincent de Montpréville,[1,6] Olaf Mercier,[6] Pierre Validire,[7] Jean-Yves Scoazec,[5] Christophe Massard,[8] Salem Chouaib,[1] David Planchard,[2] Julien Adam,[1,9] Benjamin Besse,[2,9] and Fathia Mami-Chouaib[1,11,*]

[1]INSERM UMR 1186, Integrative Tumor Immunology and Immunotherapy, Gustave Roussy, Faculté de Médecine, Université Paris-Sud, Université Paris-Saclay, 94805 Villejuif, France

[2]Department of Cancer Medicine, Gustave Roussy, Institut d'Oncologie Thoracique, Gustave Roussy, Université Paris-Saclay, 94805 Villejuif, France

[3]Gastrointestinal and Medical Oncology Department, Hôpital Européen Georges Pompidou, Paris, France

[4]INSERM Unit U981, Department of Experimental Pathology, Gustave Roussy, Université Paris-Sud, Université Paris-Saclay, 94805 Villejuif, France

[5]Department of Biology and Medical Pathology, Gustave Roussy, 94805 Villejuif, France

[6]Hôpital Marie-Lannelongue, Service d'Anatomie Pathologique, 92350 Le-Plessis-Robinson, France

[7]Institut Mutualiste Montsouris, Service d'Anatomie Pathologique, 75014 Paris, France

[8]Drug Development Department, Gustave Roussy, Université Paris-Saclay, 94805 Villejuif, France

[9]These authors contributed equally

[10]Present address: Laboratory of Translational Genomics and Targeted Therapeutics in Solid Tumors, August Pi i Sunyer Biomedical Research Institute (IDIBAPS), and Medical Oncology Department, Hospital Clínic, Barcelona, Spain

[11]Lead Contact

*Correspondence: fathia.mami-chouaib@gustaveroussy.fr

https://doi.org/10.1016/j.xcrm.2020.100127

SUMMARY

Accumulation of CD103$^+$CD8$^+$ resident memory T (T_{RM}) cells in human lung tumors has been associated with a favorable prognosis. However, the contribution of T_{RM} to anti-tumor immunity and to the response to immune checkpoint blockade has not been clearly established. Using quantitative multiplex immunofluorescence on cohorts of non-small cell lung cancer patients treated with anti-PD-(L)1, we show that an increased density of CD103$^+$CD8$^+$ lymphocytes in immunotherapy-naive tumors is associated with greatly improved outcomes. The density of CD103$^+$CD8$^+$ cells increases during immunotherapy in most responder, but not in non-responder, patients. CD103$^+$CD8$^+$ cells co-express CD49a and CD69 and display a molecular profile characterized by the expression of PD-1 and CD39. CD103$^+$CD8$^+$ tumor T_{RM}, but not CD103$^-$CD8$^+$ tumor-infiltrating counterparts, express Aiolos, phosphorylated STAT-3, and IL-17; demonstrate enhanced proliferation and cytotoxicity toward autologous cancer cells; and frequently display oligoclonal expansion of TCR-β clonotypes. These results explain why CD103$^+$CD8$^+$ T_{RM} are associated with better outcomes in anti-PD-(L)1-treated patients.

INTRODUCTION

Effective cancer immunotherapy requires the generation of persistent tumor-reactive cytotoxic T lymphocytes (CTLs) that continuously eliminate primary malignant cells and micro-metastases. Immune checkpoint blockade (ICB), in particular via anti-programmed cell death-1 (PD-1) and anti-PD-L1 neutralizing monoclonal antibodies (mAbs), has led to improved outcomes in non-small cell lung cancer (NSCLC) patients by blocking the interaction of PD-1 inhibitory receptor on tumor-specific T cells with its ligand PD-L1 on target cells, thereby reactivating their anti-tumor effector functions. ICB, as a single immunotherapy agent, has demonstrated responses in up to 20% of patients with advanced NSCLC who failed platinum-based chemotherapy. In this context, the clinical benefits of anti-PD-(L)1 therapy require that tumors be infiltrated by CD8$^+$ T lymphocytes expressing high levels of PD-1 and mediating tumor mutation-derived neoantigen-specific responses.[1,2] However, little is known of the nature of these CD8$^+$ T lymphocytes, whether they belong to the memory pool of T cells, and whether they patrol through blood or are confined to tumor tissues, where they are permanently retained. Recently, a lineage of CD8$^+$ memory T cells, called resident memory T (T_{RM}) cells, was localized in several human

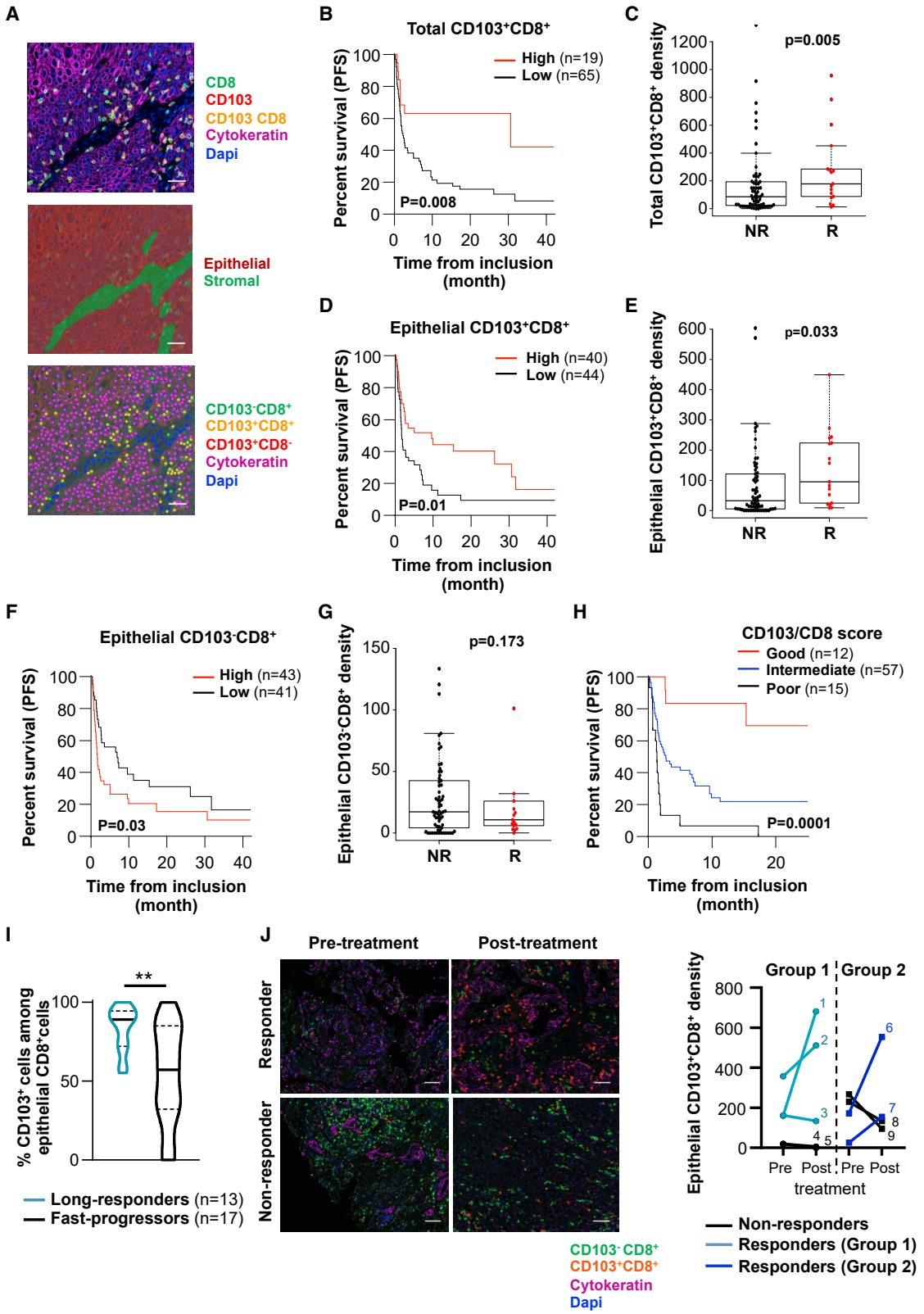

(legend on next page)

solid tumors, including NSCLC, and was associated with a favorable prognosis.[3–8]

T_{RM} cells were initially identified in infectious diseases, where they were located at sites of pathogen entry so as to trigger optimized protection against viral re-infections.[9] They are distinct from central memory T (T_{CM}) and effector memory T (T_{EM}) cells due to their non-recirculating behavior and restricted localization in non-lymphoid peripheral tissues. This memory T cell subset lacks molecules such as S1pr1, Klf2, CCR7, and CD62L, enabling egress from tissue and migration to lymph nodes, and has a unique surface phenotype characterized by the expression of the CD69 activation marker and CD103 (α_E(CD103) β_7) and CD49a (α_1(CD49a) β_1) integrins, which likely participate in their residency feature by binding to E-cadherin and type IV collagen on epithelial and endothelial cells, respectively.[10,11] T_{RM} cells also upregulate lymphocyte function-associated antigen-1 (LFA-1 or α_L(CD11a) β_2) integrin, which sustains their residence in liver tissue by binding to intercellular adhesion molecule-1 (ICAM-1) on endothelial cells.[12] Formation and persistence of antiviral T_{RM} are regulated by a specific repertoire of transcription factors, including Runx3, Blimp-1, Hobit (homolog of Blimp-1 in T cells), and Notch, and involve a specific set of cytokines, including transforming growth factor β (TGF-β), interleukin-15 (IL-15), type I interferon (IFN), and IL-12.[13–15] T_{RM} have been shown to produce pro-inflammatory cytokines such as IFN-γ and tumor necrosis factor (TNF) and cytotoxic serine protease granzyme B, which participate in recruiting other immune cells at the sites of infection and mediating cytotoxic function, respectively. With regard to cancer diseases, much less is known about the generation and maintenance of T_{RM} at the tumor site and their role in anti-tumor immune responses. Thus far, the phenotypic and functional features of human tumor T_{RM} cells and their contribution to T cell immunity to cancer and responses to ICB are poorly understood. In this report, we show that human lung tumor $CD8^+$ T_{RM} cells are a homogeneous $CD103^+CD49^+CD69^+$ population characterized by the expression of T-bet, phosphorylated (p)STAT-3, and Aiolos transcription factors, and that a subset of them produces IFN-γ and IL-17, specific to Tc17 cells. NSCLC $CD8^+$ T_{RM} cells also produce granzyme B, form stable conjugates with autologous tumor cells, and mediate specific cytotoxic activity toward the cognate target. This tumor T_{RM} subset, but not its $CD103^-CD8^+$ tumor-infiltrating counterpart, proliferate and clonally expand in some tumors, suggesting that it is enriched in tumor-specific $CD8^+$ T cells. Remarkably, an enhanced $CD103^+CD8^+$ subset within the tumor microenvironment (TME) is associated with better progression-free survival (PFS) of anti-PD-(L)1-treated NSCLC patients. This subset is increased upon anti-PD-1 administration in tumors from most responder patients, but not in tumors from non-responder patients, and represents the major $CD8^+$ tumor-infiltrating lymphocytes (TILs) population in intraepithelial tumor regions. Thus, $CD103^+CD8^+$ T_{RM} cells could be considered potential biomarkers when selecting patients who may benefit from ICB.

RESULTS

Accumulation of $CD103^+CD8^+$ Cells in Tumors Is Associated with Better Outcomes in Anti-PD-(L)1-Treated NSCLC Patients

To determine the contribution of T_{RM} cells to the response to ICB, we established a retrospective tumor cohort (discovery cohort) of 111 patients with advanced NSCLC treated with single-agent anti-PD-(L)1 mAbs (Table S1). Tumor sections from formalin-fixed, paraffin-embedded (FFPE) samples were stained simultaneously with anti-CD8, anti-CD103, and anti-cytokeratin mAbs, and the density and distribution of $CD103^+CD8^+$ TIL and $CD103^-CD8^+$ TIL in epithelial and stromal regions were assessed using InForm software (Figure 1A). Among the 111 analyzed tumor samples, conclusive staining for the quantification of $CD103^+CD8^+$ TIL was obtained for 86 patients. Multiplex fluorescent immunohistochemistry (IHC) revealed that the

Figure 1. Increased $CD103^+CD8^+$ TILs Are Associated with Improved Outcomes of Anti-PD-1-Treated NSCLC

(A) Fluorescent IHC image of CD8, CD103, cytokeratin, and DAPI staining in lung tumor section (top). Digital markup image shows epithelial and stromal zones of the tumor section defined by cytokeratin staining (center). Digital markup image shows $CD103^+CD8^+$ (yellow), $CD103^-CD8^+$ (green), $CD103^+CD8^-$ (red), and $cytokeratin^+$ (pink) cells in lung tumors (bottom). Scale bar, 2 cm.

(B) Kaplan-Meier curve shows iPFS of anti-PD-1-treated patients with tumors harboring high (>252/mm^2) (n = 19) or low (<252/mm^2) (n = 65) densities of $CD103^+CD8^+$ cells (n = 84).

(C) Density of total $CD103^+CD8^+$ cells in tumors depending on iORRs of non-responders (NR) (n = 65) and responders (R) (n = 17) patients to PD-1 blockade.

(D) Kaplan-Meier curve shows iPFS of anti-PD-1-treated patients with tumor epithelial regions harboring a high (>48/mm^2) (n = 40) or low (<48/mm^2) (n = 44) density of $CD103^+CD8^+$ cells (n = 84).

(E) Density of $CD103^+CD8^+$ cells in epithelial tumor regions depending on iORRs of NR (n = 65) and R (n = 17) patients to anti-PD-1.

(F) Kaplan-Meier curve shows iPFS of PD-1 blockade-treated patients with epithelial regions of tumors harboring a high (>17/mm^2) (n = 43) or low (<17/mm^2) (n = 41) density of $CD103^-CD8^+$ cells.

(G) Density of $CD103^-CD8^+$ cells in epithelial tumor regions depending on iORRs of NR (n = 65) and R patients (n = 17) to PD-1 blockade.

(H) Kaplan-Meier curve shows iPFS of anti-PD-1-treated patients with tumors harboring a satisfactory ($CD103^+CD8^{+high}$/$CD103^-CD8^{+low}$, red, n = 12), intermediate ($CD103^+CD8^{+high}$ or $CD103^-CD8^{+low}$, blue, n = 57), or poor ($CD103^+CD8^{+low}$/$CD103^-CD8^{+high}$, black, n = 15) CD103/CD8 score.

(I) Percentages of $CD103^+$ cells among $CD8^+$ TILs in epithelial tumor areas of anti-PD-1-treated patients undergoing a long-response (PFS > 6 months and OS > 12 months; n = 13) or a fast-progression (OS < 12 weeks; n = 17). **p < 0.01.

(J) Fluorescent IHC images show $CD103^+CD8^+$ (orange), $CD103^-CD8^+$ (green), $cytokeratin^+$ (pink), and $DAPI^+$ (blue) cells in tumors from responder and non-responder patients before and after administration of anti-PD-1. Scale bar, 1 cm. Right, density of $CD103^+CD8^+$ cells in epithelial tumor regions of tumors before and after the administration of anti-PD-(L)1 in responder (n = 5) or non-responder (n = 4) patients.

Each symbol represents an individual patient; horizontal lines correspond to mean ± standard deviation (SD) (C, E, and G). p value was determined by log-rank test (B, D, F, and H), Chi-square test (C, E, and G) or unpaired t test (I).

See also Figures S1 and S2, and Tables S1–S6.

density of the $CD103^+CD8^+$ TIL subset varied between tumors, ranging from 0 to 1,320 cells/mm^2, with a median of 103 cells/mm^2. Most $CD103^+CD8^+$ TILs were located within the stroma, with a median density of 153 cells/mm^2. In epithelial tumor regions, there were fewer lymphocytes than in the stroma (median density of 68 cells/mm^2); however, 76% of these $CD8^+$ TILs were $CD103^+$ (median density of 45 cells/mm^2), whereas only 48% in the stroma (Table S1). Increased intraepithelial lymphocyte infiltration was particularly observed in tumors with a high density of $CD103^+CD8^+$ cells in the stromal compartment (Figure S1A).

We then correlated the survival of patients from the date of the first immunotherapy administration with the score of tumor infiltration by $CD8^+$ TILs. In this cohort, the objective response rate (ORR) was 20% (n = 17/86), corresponding to responders. As expected, patients with strong CD8 cell ($CD8^{high}$) tumor infiltration had increased survival compared to patients with $CD8^{low}$ tumors (hazard ratio [HR] = 0.40, 95% confidence interval [CI] 0.20–0.77, p = 0.006), and median immunotherapy progression-free survival (iPFS) of 9.92 months (95% CI 2.73–not reached) (Figure S1B; Table S2). The density of $CD8^+$ TIL was also higher in responder patients than in non-responders (Figure S1C). Remarkably, when patients were stratified by their tumor $CD103^+CD8^+$ cell infiltration, iPFS dramatically increased in the patient population harboring tumors that were strongly infiltrated by $CD103^+CD8^+$ cells ($CD103^+CD8^{+high}$), with median iPFS reaching 30 months (95% CI 2.73–not-reached) (Figure 1B and Table S2). The density of total $CD103^+CD8^+$ TILs also correlated with the ORR (Figure 1C). In contrast, patients with tumors slightly infiltrated by $CD103^+CD8^+$ cells had only a 2.3-month (95% CI 1.68–5.03) median iPFS. Multivariate analyses showed that tumor infiltration by $CD103^+CD8^+$ cells was an independent factor in satisfactory prognosis, based on iPFS, with a HR of 0.39 (95% CI 0.18–0.85, p = 0.01) (Table S3). More important, median iPFS in the $CD103^+CD8^{+high}$ population was 20 months longer than in the total $CD8^{+high}$ population (Table S2). As expected, PD-L1 expression by tumor cells correlates with a better PFS (Table S1). These results highlight the strong benefit of an enhanced $CD103^+CD8^+$ cell subset in tumors compared to the heterogeneous $CD8^+$ subset in the response to anti-PD-(L)1.

Correlation between Intraepithelial $CD103^+CD8^+$ TILs, Tumor E-Cadherin, and ICAM-1 Expression and Response to ICB

Next, we examined $CD8^+$ TILs in epithelial tumor regions where immune cells are in close contact with tumor cells. Patients with high intraepithelial $CD103^+CD8^+$ TILs responded more effectively to anti-PD-(L)1 than patients with low intraepithelial $CD103^+CD8^+$ infiltration (HR = 0.52, 95% CI 0.31–0.88, p = 0.01) (Figure 1D). The density of intraepithelial $CD103^+CD8^+$ TILs also correlated with the ORR (Figure 1E). Similar results were observed when analyzing total $CD8^+$ cell infiltrate in the epithelial compartment, predominantly composed of $CD103^+$ $CD8^+$ TILs (Figures S1D and S1E). Correlation between an enhanced total (Figures S1F and S1G), but to a lesser extent epithelial (Figures S1H and S1I), $CD103^+CD8^+$ subset with better PFS of anti-PD-(L)1-treated patients was confirmed in a second cohort (validation cohort) of 41 NSCLC, including 10 (26%) responder patients (Table S4). In contrast, patients with increased intraepithelial $CD103^-CD8^+$ TIL did not respond efficiently to anti-PD-1, with a HR of 1.74 (95% CI 1.05–2.88, p = 0.03), and no correlation was observed between the density of intraepithelial $CD103^-CD8^+$ cells and the ORR (Figures 1F and 1G). Since epithelial tumor region infiltration by either high numbers of $CD103^+CD8^+$ cells or low numbers of $CD103^-CD8^+$ cells was associated with better outcomes, we stratified the cohort into 3 groups based on these 2 parameters. Using a CD103/CD8 score, we considered a group satisfactory if both parameters were present ($CD103^+CD8^{+high}$ and $CD103^-$ $CD8^{+low}$), intermediate if only 1 parameter was present ($CD103^+CD8^{+high}$ or $CD103^-CD8^{+low}$), and poor if neither was present ($CD103^+CD8^{+low}$ and $CD103^-CD8^{+high}$). Interestingly, the group with a satisfactory CD103/CD8 score had a median PFS of 26.2 months (95% CI 15.3–not-reached) versus 2.7 months (95% CI 1.7–7.3) for the group with an intermediate score and 1.38 months for the group with a poor score (95% CI 0.72–1.97, p < 0.0001) (Figure 1H; Table S2). In addition, anti-PD-1-long-responder patients (PFS > 6 months and overall survival [OS] > 12 months) displayed a higher frequency of $CD103^+$ cells among $CD8^+$ TILs than fast-progressor patients (defined by an "early death" occurring during the first 12 weeks after the beginning of ICB) (Figure 1I). A higher density of intraepithelial $CD103^+CD8^+$ TILs in anti-PD-1-long-responder patients than in fast-progressor patients was also obtained in the validation cohort (Figure S1J). More important, quantitative multiplex fluorescent IHC staining of tumors collected from 9 patients (5 from the validation cohort and 4 additional patients) before (2–25 weeks) and after anti-PD-1 administration showed an increase in the density of epithelial $CD103^+CD8^+$ TILs in 4 of 5 responder patients. In contrast, no expansion of this subset was observed in 4 of 4 non-responder patients (Figure 1J; Table S5). An increase in total $CD103^+CD8^+$ and total $CD8^+$ TILs was also observed in responder patients (Table S5). These results highlight the importance of enhanced intratumoral $CD103^+$ $CD8^+$ cells in response to anti-PD-(L)1 and support the conclusion of a role of this subset in patient outcomes.

We then assessed the expression of E-cadherin and ICAM-1, the respective ligands of CD103 and LFA-1 integrins, known to play a major role in strengthening the interaction between CTLs and tumor cells following T cell receptor (TCR) recognition of major histocompatibility complex (MHC) class I-peptide complexes.[16,17] The expression of E-cadherin on cancer cells from 105 evaluable tumor sections of the 111 analyzed NSCLCs was scored into 4 groups: scores 0 and 1 were considered low (12%, n = 13/105) and scores 3 and 4 were high (88%, n = 92/105) (Figure S2A; Table S6). Data analyses indicated that E-cadherin expression does not affect PFS, and no effect on the density of intraepithelial $CD103^+CD8^+$ TILs was observed (Figures S2B and S2C). Similarly, according to ICAM-1 expression on tumor cells from 101 evaluable tumor sections of the 111 analyzed tumors, the population was classified into low and high groups (Figure S2D), with no impact observed on survival or infiltration by $CD103^+CD8^+$ cells in epithelial regions (Figures S2E and S2F). Nevertheless, for tumors combining an epithelial $CD103^+CD8^{+high}$ plus ICAM-1^{high} profile, median PFS increased up to 15.3 months (95% CI 9.63–not reached) versus a median PFS of 3.8 months (95% CI 2.56–not reached) observed for the

epithelial CD103^{+}CD8^{+high} plus ICAM-1^{low} profile (Figure S2G; Table S2). These results support the observation that CD103 promoted CD8 T cell infiltration within epithelial tumor regions, and suggest that these CD103^{+}CD8^{+} lymphocytes are tumor-reactive T_{RM} cells.

CD8^{+} TILs from NSCLC Are Highly Enriched in CD103^{+}CD49a^{+}CD69^{+} T_{RM}

Experiments were next performed to delineate the phenotypic and molecular features of CD103^{+}CD8^{+} NSCLC TILs, and to determine whether they are a homogeneous population or whether heterogeneity exists in the expression of conventional T_{RM} surface markers. With this aim, CD8^{+} TILs from 39 freshly resected treatment-naive early-stage NSCLC tumors were isolated and stained for CD3, CD8, CD103, CD49a, and CD69, as well as the effector T cell (T_{Eff}) surface marker KLRG1 (Figure S3A). The results indicated that the percentage of CD8^{+} T cells displaying a CD103^{+}KLRG1^{-} phenotype ranged from 18% to 81%, with a mean of 51%, while the percentage of CD8^{+} T cells displaying a CD103^{-}KLRG1^{+} T_{Eff} phenotype ranged from 7% to 52%, with a mean percentage of 26% (Figure 2A). The mean percentages of CD103^{+}KLRG1^{+} and CD103^{-}KLRG1^{-} T cell subpopulations were only ~10% and 12% of CD8^{+} TILs, respectively. Notably, the expression of CD103 inversely correlated with that of KLRG1 on CD8^{+} TILs and appeared mutually exclusive (Figure 2B).

We then further characterized the CD103^{+}CD8^{+} TIL subset by evaluating the expression of CD69 and CD49a T_{RM} markers. The results showed that >90% of CD103^{+}CD8^{+} T cells expressed CD69 and CD49a (Figures 2C, S3A, and S3B), and that the expression of CD49a correlated with that of CD103 (Figure 2D). In addition, most CD103^{+} TILs displayed a CCR7^{-}CD45RA^{-} profile, which is characteristic of T_{EM} cells (Figure S3C). In contrast, only 50% and 35% of KLRG1^{+}CD8^{+} TILs expressed CD69 and CD49a, respectively (Figure 2C). This T cell subset is more heterogeneous in CD45A expression and is mainly composed of CCR7^{-}CD45RA^{-} T_{EM} and CCR7^{-}CD45RA^{high} terminally differentiated (EMRA) T cells (Figure S3C). CD103^{+}CD49a^{+}CD69^{+} CD8 T cells, hereafter called T_{RM} cells are also present in adjacent healthy lung tissues, but at a lower frequency and lower expression level of CD69 than in autologous tumor tissues (Figures 2E and 2F). In contrast, the KLRG1^{+} CD8 T cell subset, hereafter referred to as non-T_{RM} cells, is more abundant in healthy lung tissue than in the cognate tumor (Figure 2E). In addition, the number of T_{RM} cells per milligram of tissue is much higher in the tumor than in the cognate normal lung, with mean values of ~1,000 T_{RM}/mg of tumor versus 100 T_{RM}/mg of healthy lung (Figure 2G), with no correlation between the 2 tissue compartments within each patient sample (Table S7). These data support the conclusion that NSCLCs are strongly infiltrated by a homogeneous CD103^{+}CD49a^{+}CD69^{+} CD8 T_{RM} subset, which is readily distinguishable from the KLRG1^{+} CD8 T_{Eff} subset.

Molecular Features of NSCLC CD8 T_{RM} Cells

To determine the transcriptional profile of the tumor T_{RM} subset, we performed RNA-based next-generation sequencing (RNA-seq) of CD103^{+}CD8^{+} and matched KLRG1^{+}CD8^{+} T cells freshly isolated from the TILs of 7 treatment-naive early-stage NSCLCs. Gene expression analyses performed with $p \leq 0.05$ revealed a large number of transcripts (n = 2,958) differentially expressed in the 2 T cell subsets, supporting the notion that they correspond to 2 divergent populations (Figure S3D). Among these transcripts, we identified a gene signature that is characteristic of antiviral T_{RM} cells and NSCLC T cells,[5,13,18,19] including the upregulation of *CXCR6* and *SIRPG* transcripts (Figure S3E; Table S8). A gene signature with the upregulation of *GPR34*, *ITGAE*, and *CXCR6* genes and the downregulation of *SIPR5* and *SIPR1*, encoding sphingosine phosphate receptors, *KLF2*, encoding Krüppel-like transcription factors that regulate T cell trafficking, and *SELL,* encoding L-selectin CD62L, important in lymphocyte homing to lymphoid organs, was identified in tumor T_{RM} cells (Figure S3F; Table S8). The downregulation of S1pr1 in tumor CD103^{+}CD8^{+} T_{RM} cells was confirmed by multiparametric flow cytometry, with levels similar to those of healthy lung T_{RM} cells (Figure S3G). In addition, gene set enrichment analysis (GSEA) showed that several hallmark gene sets, such as inflammation, cell cycle, TGF-β signaling pathways, mammalian target of rapamycin (mTOR), and hypoxia, were enriched in T_{RM} cells (Figures S4A and S4B; Table S9).

Among T_{RM} signature genes, a panel of genes involved in T cell exhaustion, including *CTLA-4*, *BTLA*, *HAVCR2*, *PDCD1*, *LAG3*, and *TIGIT*, were more strongly expressed in CD103^{+} than in KLRG1^{+} TIL subsets (Figures 3A and S4C; Table S8). The upregulation of *SPRY1* (Sprouty), *ENTPD1* (CD39), *LAYN* (Layilin), and *TOX* genes was also observed in T_{RM} cells (Figure S4C). Flow cytometry analyses confirmed enhanced expression of PD-1 on T_{RM} cells from tumors, but not on non-T_{RM} cells and T_{RM} cells from cognate healthy lung tissue (Figure 3B). Notably, ectonucleotidase CD39 was specifically expressed by T_{RM} cells, and its expression was associated with PD-1 (Figures 3C and S4D). Moreover, t-distributed stochastic neighbor embedding (t-SNE) analysis highlighted the strong correlation of expression of CD39 and PD-1 with the T_{RM} cluster, whereas the non-T_{RM} cluster showed a weak association with these markers (Figure 3D). The expression levels of CD103 on CD8^{+} TILs correlated with CD39 and 4-1BB (CD137) levels, and CD103^{high} T cells also displayed CD39^{high} (Figure 3E) and 4-1BB^{high} (Figure 3F) expression profiles characteristic of antigen-experienced T lymphocytes.[20,21] As expected, T_{RM} cells from adjacent normal lung expressed only low levels of 4-1BB, excluding the recent engagement of TCR with specific antigen (Figure 3F). These results support the hypothesis that NSCLC CD103^{+}CD8^{+} TILs were enriched with tumor-reactive T cells harboring all of the features of activated T_{RM} cells.

Lung Tumor T_{RM} Cells Express Transcription Factors Involved in Th17 Differentiation

To explore potential pathways involved in T_{RM} formation in tumors, we studied genes encoding transcription factors differentially expressed in CD103^{+}CD8^{+} and KLRG1^{+}CD8^{+} TILs. RNA-seq analyses indicated that CD103^{+}CD8^{+} T cells displayed a specific signature characterized by the upregulation of *ZEB1* encoding the zinc-finger E-box binding homeobox-1, *ZNF683* (zinc finger 683) encoding the Blimp1 homolog Hobit, and *PRDM1* (BLIMP1), and the downregulation of *EOMES*, *IKZF2* (*HELIOS*), and *TCF7* genes (Figures 4A, 4B, and S5A; Table S8).

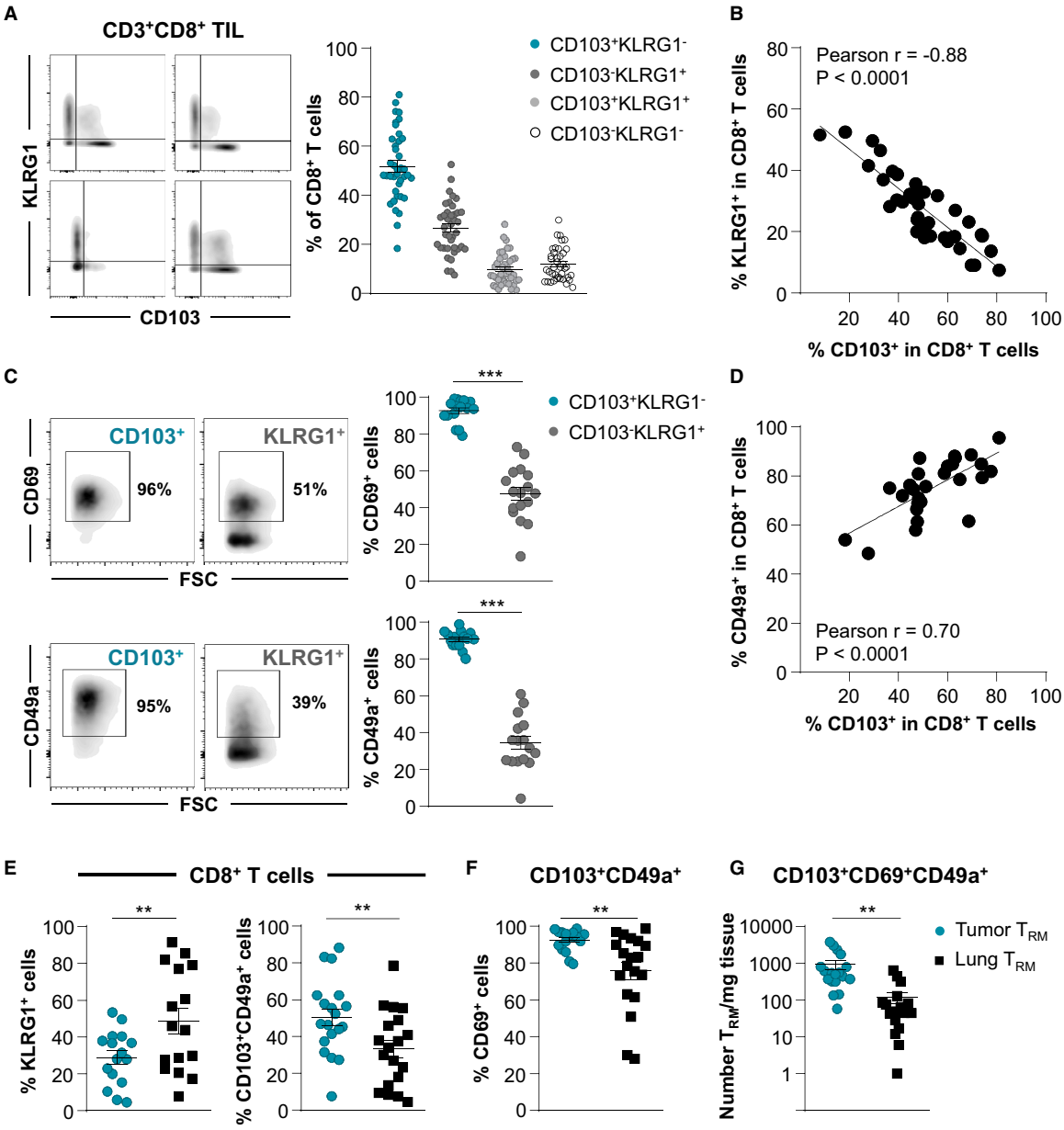

Figure 2. Expression of CD103, CD49a, and CD69 on CD8 T Cells Infiltrating Treatment-Naive NSCLC and Healthy Lung Tissues

(A) Freshly resected NSCLC tumors were dissociated and the $CD8^+$ T cell subset was analyzed for CD103 and KLRG1 expression. Representative dot plots from 4 different TIL samples are included (bi-exponential scale). Right, percentages of $CD103^+KLRG1^-$, $CD103^-KLRG1^+$, $CD103^+KLRG1^+$, and $CD103^-KLRG1^-$ TIL subsets among $CD3^+CD8^+$ cells (n = 39).

(B) Inverse correlation between percentage of $CD103^+$ and $KLRG1^+$ cells among $CD8^+$ TILs (n = 40). The r value indicates Pearson correlation coefficient.

(C) Expression of CD69 and CD49a on $CD103^+$ and $KLRG1^+$ $CD8^+$ TILs. Representative dot plot from 1 TIL sample is shown. Right, percentages of $CD69^+$ and $CD49a^+$ cells among $CD103^+$ and $KLRG1^+$ CD8 TILs are presented (n = 17 and n = 16, respectively).

(D) Correlation between percentage of $CD103^+$ and $CD49a^+$ cells among $CD8^+$ TIL (n = 27). The r value indicates Pearson correlation coefficient.

(E) Percentages of $KLRG1^+$ (n = 16) and $CD103^+CD49^+$ cells (n = 19) among $CD8^+$ T cells infiltrating tumors or autologous healthy lung tissues.

(F) Percentages of $CD69^+$ cells among $CD103^+CD49a^+$ CD8 T cells from tumor or healthy lung tissues (n = 19).

(G) Total numbers of $CD103^+CD69^+CD49a^+$ CD8 (T_{RM}) cells per milligram of tumor tissues and paired normal lung tissues (n = 18).

Each symbol represents individual TILs or lung sample; horizontal lines correspond to means ± standard errors of the mean (SEM). $^{**}p < 0.01$, $^{***}p < 0.001$ (paired t test).

See also Figure S3 and Table S7.

CellPress
OPEN ACCESS

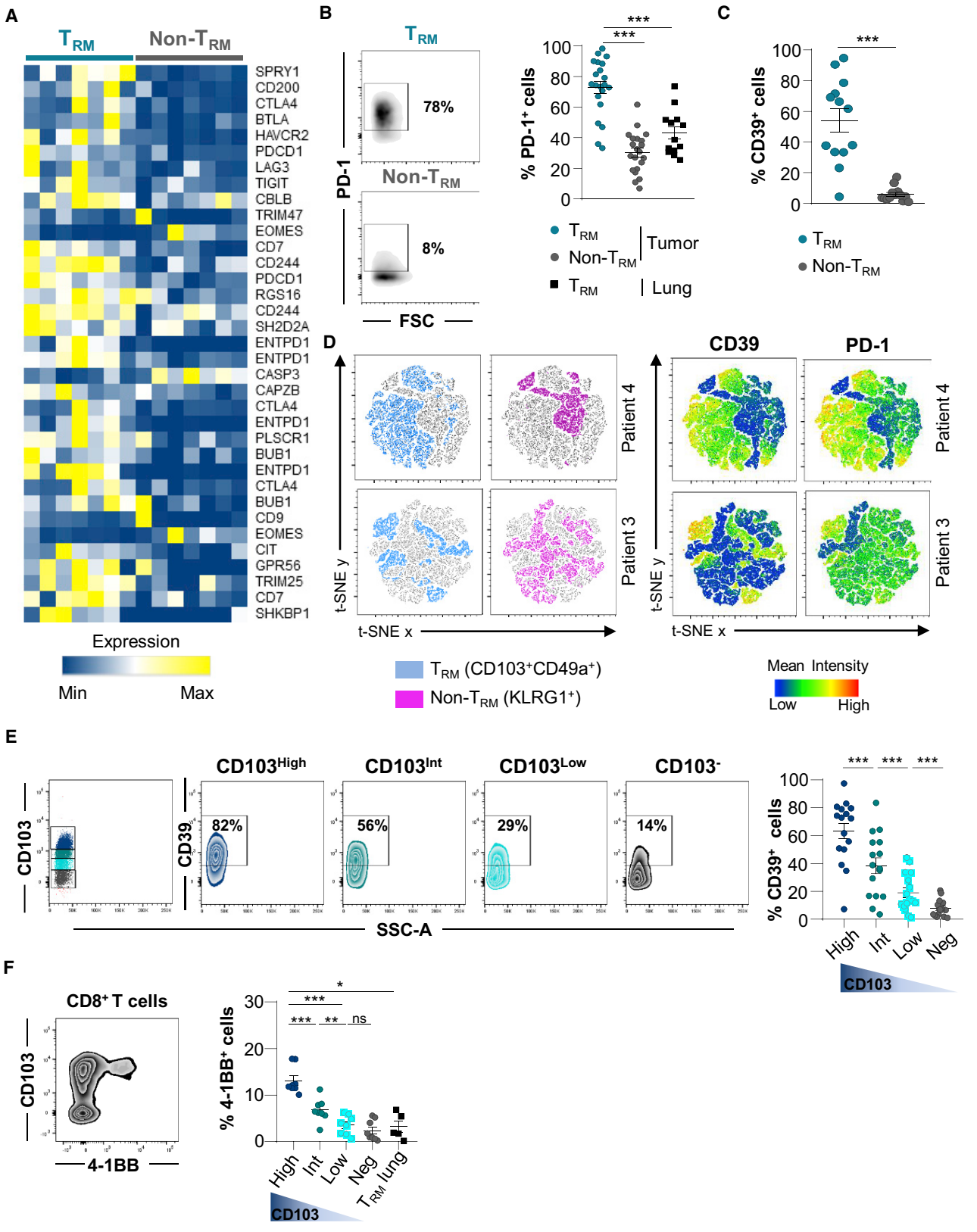

(legend on next page)

Remarkably, a set of genes encoding transcription factors involved in Th17 differentiation, such as *IKZF3* encoding the Ikaros transcription factor family member Aiolos, and *AHR* encoding an aryl hydrocarbon receptor, were more strongly expressed in T_{RM} cells than in non-T_{RM} cells (Figure 4B and S5A). A panel of genes associated with the Aiolos pathway, including *SMARCA4*, *UBE2I*, and *GRAP2*, were also upregulated in T_{RM} cells (Figure S5B).

Flow cytometry analyses showed that tumor T_{RM} cells expressed lower levels of Hobit protein than non-T_{RM} cells, but levels higher than in healthy lung T_{RM} cells (Figure 4C). The downregulation of the *TCF7* gene-encoding protein TCF-1 in tumor T_{RM} as compared to non-T_{RM} cells was confirmed at the protein level (Figure 4D). In contrast, T-bet and Aiolos transcription factors were more strongly expressed in tumor T_{RM} than in non-T_{RM} cells, at levels similar to or higher than those in healthy lung T_{RM} cells (Figure 4E). Moreover, AhR protein and phosphorylated-STAT3 (pSTAT3), also known as the master regulators of Th17 differentiation, were more strongly expressed in T_{RM} than in non-T_{RM} cells, and at levels similar to those of healthy lung T_{RM} cells (Figures 4F, 4G, and S5C). Notably, tumor T_{RM} cells displaying high levels of CD103 ($CD103^{high}$) expressed higher levels of pSTAT3 than T_{RM} cells with intermediate ($CD103^{Int}$) and low ($CD103^{low}$) CD103 expression (Figure 4G). In addition, tumor T_{RM} cells expressed similar levels of pSTAT3 and Aiolos than healthy donor $Th17^+$ control cells (Figures 4E and 4G). In contrast, AhR was more strongly expressed in $Th17^+$ controls than in tumor T_{RM} cells (Figure 4F). The transcription factor RORγt was equally expressed by T_{RM} and non-T_{RM} cells, and the chemokine receptor CCR6 was more strongly expressed in T_{RM} than in non-T_{RM} cells (Figure S5D; Table S8). These results demonstrate that, together with T-bet, human lung tumor $CD8^+$ T_{RM} cells express Aiolos, AhR, and pSTAT3, three master regulators of the Th17 pathway, and ultimately suggest that they are enriched with Tc17 lymphocytes.

Lung Tumor $CD8^+$ T_{RM} Cells Contain Tc17 and are Tumor-Reactive CTL

To gain further insight into the molecular characteristics of human lung tumor $CD8^+$ T_{RM} cells, we studied the expression profiles of genes involved in T cell activation. The results showed that T_{RM} displayed a signature of more activated lymphocytes than non-T_{RM} cells (Figure 5A). Notably, GSEA highlighted the upregulation of several genes belonging to the Th17/Tc17 cell lineage in T_{RM} cells (Figure 5B; Table S8). Among these genes, *IL17A* and *IL17RA*, encoding IL-17 and the IL-17 receptor (IL-17R), were more strongly expressed in T_{RM} than in non-T_{RM} cells (Figure 5C; Table S8). The upregulation of *IL17A* transcript in some T_{RM}, but not in non-T_{RM} cells, was further confirmed by qRT-PCR using paired $CD103^+CD8^+$ and $KLRG1^+CD8^+$ T cells from 6 additional lung TILs (Figure S5E). Moreover, intracellular flow cytometry analysis of fresh TILs stimulated *ex vivo* with phorbol myristate acetate (PMA) plus ionomycin showed production of IL-17 by T_{RM} cells and healthy donor $Th17^+$ control cells, but not by non-T_{RM} cells (Figure 5D). Remarkably, higher percentages of IL-17-producing cells were observed in $CD103^{high}$ T_{RM} cells than in $CD103^{int}$ and $CD103^{low}$ cells (Figure S5F), and the expression of CD39 and 4-1BB was frequently higher in $IL\text{-}17^+$ than in $IL\text{-}17^-$ T_{RM} cells (Figure S5G). ELISA also confirmed the restricted secretion of IL-17 in supernatants from T_{RM}, but not from non-T_{RM} cells (Figure 5E). In contrast, both non-T_{RM} and T_{RM} cells from tumors were able to produce high levels of IFN-γ and TNF-α following *ex vivo* stimulation with PMA plus ionomycin (Figure 5F). Moreover, a subset of T_{RM} cells from lung tumors produced both IL-17 and IFN-γ (Figure 5G). These IL-17-producing $CD8^+$ T cells were not TCR-γδ lymphocytes, which often display a $CD4^-CD8^-$ profile and represent ~3.6% of $CD3^+$ TILs, and only 2.2% of them produced IL-17 (Figures S5H and S5I).

Flow cytometry analyses showed that tumor T_{RM} cells expressed higher levels of proliferation marker protein Ki67 compared to tumor non-T_{RM} and T_{RM} cells from adjacent healthy lung (Figure 6A). Intracellular immunofluorescence also revealed that tumor T_{RM} cells expressed higher levels of granzyme B than non-T_{RM} and healthy lung T_{RM} cells, supporting the hypothesis that they are tumor-reactive CTLs (Figure 6B). Consistently, further functional studies by confocal microscopy showed that tumor T_{RM} cells formed more stable conjugates with autologous cancer cells than non-T_{RM} cells, as evaluated by tyrosine phosphorylation (pTyr) at the contact zone between T cells and target cells (Figure 6C). Moreover, tumor T_{RM} cells

Figure 3. Expression of T Cell Exhaustion Hallmark in T_{RM} Cells from NSCLC Tumors

(A) Heatmap of transcripts involved in T cell exhaustion differentially expressed in $CD103^+$ and $KLRG1^+$ $CD8^+$ TILs (n = 7). Different expression patterns correspond to different isoforms of the same gene.

(B) Expression of PD-1 on $CD103^+$ and $KLRG1^+$ $CD8^+$ TILs. Dot plots of 1 representative patient. Right, percentages of $PD\text{-}1^+$ cells among T_{RM} and non-T_{RM} (n = 21) and paired T_{RM} from healthy lung (n = 13).

(C) Percentages of $CD39^+$ cells in paired T_{RM} and non-T_{RM} from NSCLCs (n = 13).

(D) t-SNE map of $CD103^+CD49a^+$ (blue) and $KLRG1^+$ (pink) cells among $CD8^+$ TILs. Right, t-SNE analysis of CD39 and PD-1 expression on $CD103^+CD49a^+$ (T_{RM}) and $KLRG1^+$ (non-T_{RM}). The data are from 2 representative TIL samples (patients 3 and 4).

(E) Dot plots of CD39 expression on $CD103^+CD8^+$ T_{RM}, displaying high ($CD103^{high}$), intermediate ($CD103^{int}$), and low ($CD103^{low}$) CD103 phenotypes, and $CD103^-CD8^+$ TIL from 1 representative tumor. Right, percentages of $CD39^+$ cells among T_{RM} expressing high, intermediate, and low levels of CD103 and $CD103^-CD8^+$ TIL (n = 16).

(F) Dot plot of 4-1BB expression on $CD103^+CD8^+$ TILs from 1 representative tumor. Right, percentages of $4\text{-}1BB^+$ cells among T_{RM} displaying high, intermediate, and low CD103 profiles. $CD103^-CD8^+$ TIL (n = 7) and $CD103^+CD8^+$ T_{RM} from autologous normal lungs (n = 4) are included. CD103 intensity is shown by a gradient color code.

Symbols represent individual TILs or lung samples; horizontal lines correspond to means ± SEMs. $^*p < 0.05$, $^{**}p < 0.01$, and $^{***}p < 0.001$ (paired t test or ANOVA with Bonferroni post hoc test); ns, not significant.

See also Figures S3 and S4 and Table S8.

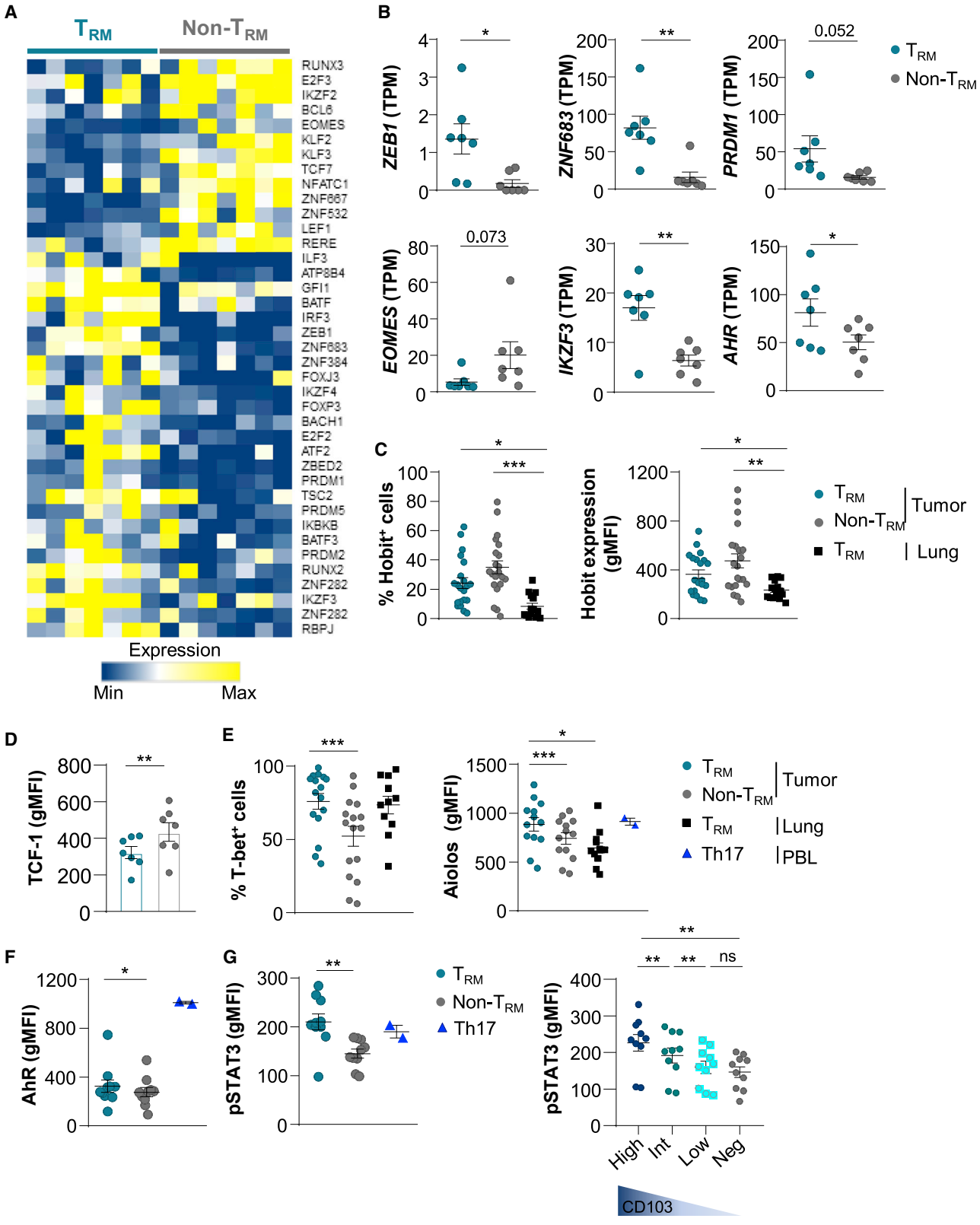

(legend on next page)

were able to kill autologous tumor cells much more efficiently than non-T_{RM} cells (Figure 6D). These results further support the conclusion that T_{RM} cells infiltrating NSCLC tumors are activated tumor-specific cytotoxic effectors.

Lung Tumor CD8$^+$ T_{RM} Cells Express a More Clonal TCR Repertoire Than Non-T_{RM} Cells

To assess the clonality of NSCLC CD8$^+$ T_{RM} cells, we investigated the TCR-β repertoire of 9 freshly sorted CD103$^+$CD8$^+$ TILs and autologous KLRG1$^+$CD8$^+$ TILs by deep TCR sequencing (TCR-seq). Results indicated that tumor T_{RM} cells were more oligoclonal than paired non-T_{RM} cells (Figures 7A and S6A). The 10 most frequent (top 10) TCR-β clonotypes, defined by hypervariable complementarity-determining region 3 (CDR3) nucleotide sequences, accounted for >60% of the T_{RM} population and <45% of the non-T_{RM} population (Figure 7B). In contrast, only a marginal difference was observed between TCR-β repertoires of T_{RM} cells from NSCLC tumors and proximal healthy lung (Figure S6B). TCRV-β (TCR variable β chain) family distribution within each T cell subset was variable across patients, but it was different between T_{RM} and non-T_{RM} cells from a given patient (Figure 7C). However, T_{RM} and non-T_{RM} populations shared some clonotypes, the proportions of which varied from one patient to another and ranged from 4% to 28% (Figures S6C–S6E). Next, we questioned whether the restricted TCR-β repertoire observed in T_{RM} cells correlated with the expression of PD-1, reported to identify the CD8$^+$ tumor-specific repertoire infiltrating human tumors.[22] The data revealed a correlation between the productive frequency of the top 10 clonotypes and the percentage of PD-1$^+$CD103$^+$CD8$^+$ TILs (Figure 7D), further supporting the conclusion that NSCLC CD8$^+$ T_{RM} cells are an oligoclonal subpopulation enriched with activated tumor-specific T cells that underwent antigen-driven expansion at the tumor site. They also explain how this tumor-resident CTL subset can locally participate in anti-tumor CD8 T cell immunity and contribute to the response to anti-PD-1 therapy.

DISCUSSION

In this report, we show that NSCLC tumors are strongly infiltrated by CD8$^+$ T_{RM} cells, most of which express a homogeneous CD103$^+$CD49a$^+$CD69$^+$ phenotype. This T_{RM} subset was also found in adjacent healthy lung tissues, but at lower densities than in autologous tumor samples, with no correlation between the frequency of either, suggesting that they are two distinct T_{RM} subsets. Tumor CD103$^+$CD8$^+$ TILs displayed transcriptomic and phenotypic signatures characteristic of T_{RM} cells, including the downregulation of (1) Klf2 (regulates genes involved in T cell trafficking such as *SELL*, *CCR7*, and *S1PR1*[23]), (2) S1pr1 (mediates the egress of T cells from lymphoid organs[24]), and (3) CD62L and CCR7 (key regulators of T cell migration to lymphoid organs) and the upregulation of (1) CD103 (favors T cell recruitment and retention in epithelial tumor islets through binding to its ligand, epithelial cell marker E-cadherin[25]), (2) CD49a (responsible for retaining CD8 T_{RM} cells in peripheral tissues via attachment to the extracellular matrix[11]), and (3) CD69 C-type lectin (modulates the T_{RM} cell capacity to exit non-lymphoid tissues through interaction and degradation of S1pr1[26]). NSCLC CD8$^+$ T_{RM} cells also overexpress several T cell inhibitory receptors and exhaustion surface markers, with co-expression of PD-1 and CD39, supporting the conclusion that they are enriched in activated tumor antigen-reactive T cells. In this regard, it has been demonstrated that PD-1 accurately identifies the repertoire of clonally expanded tumor-specific CD8$^+$ T cells.[22] The expression of CD39, together with CD103, has been reported to identify truly tumor-reactive CD8 T cells in human solid tumors[20] and to distinguish tumor antigen-specific CD8$^+$ T cells from viral antigen-specific bystander T cells present in the TME.[27] The *TOX* gene, recently identified in tumor-reactive murine T cells and in human PD1^{hi}CD39^{hi} TILs,[28] was also upregulated in human NSCLC T_{RM} cells, further indicating that they are enriched in tumor-specific T cells. NSCLC T_{RM} cells also frequently expressed 4-1BB (CD137) co-stimulatory receptor characteristics of antigen-experienced TILs.[21] These molecular features likely cooperate in retaining CD8$^+$ T_{RM} cells in tumor tissues to detect and mount robust local immune responses to transformed cells.

T-bet, together with Eomes T-box transcription factors, were demonstrated to control the development and survival of skin and lung CD103$^+$ T_{RM} cells by controlling TGF-β and IL-15 expression.[29] However, while extinguishing Eomes is necessary for CD103$^+$CD8$^+$ T_{RM} cell formation, residual T-bet expression is required for IL-15-mediated CD103$^+$CD8$^+$ T_{RM} survival. Consistently, we show that lung tumor CD103$^+$CD8$^+$ T_{RM} cells express T-bet at levels similar to healthy lung CD103$^+$CD8$^+$ T_{RM}, but they only weakly express Eomes. *ZEB1* was strongly

Figure 4. Transcription Factor Profiles of T_{RM} and non-T_{RM} from NSCLCs

(A) Heatmap of transcripts encoding transcription factors differentially expressed in CD103$^+$ and KLRG1$^+$ CD8$^+$ TIL (n = 7) ($p < 0.05$).

(B) Expression of *ZEB1*, *ZNF683* (HOBIT), *PRDM1* (BLIMP1), *IKZF3* (AIOLOS), *EOMES*, and *AHR* genes in T_{RM} and non-T_{RM} from NSCLCs (n = 7). Values are transcripts per milion (TPM).

(C) Percentages of Hobit$^+$ cells among T_{RM} and non-T_{RM} cells from NSCLCs (n = 21) and among healthy lung T_{RM} cells (n = 15). Right, expression of Hobit (gMFI) in T_{RM} and non-T_{RM} cells from NSCLCs (n = 21) and in healthy lung T_{RM} cells (n = 15).

(D) Expression of TCF-1 (gMFI) in tumor T_{RM} and non-T_{RM} cells (n = 7).

(E) Percentages of T-bet$^+$ cells among tumor T_{RM} and non-T_{RM} cells (n = 21) and among healthy lung T_{RM} cells (n = 11). Right, expression of Aiolos (gMFI) among tumor T_{RM} and non-T_{RM} and paired healthy lung T_{RM} (n = 13). Heathy donor Th17 control cells are included (n = 2).

(F) Expression of AhR (gMFI) in tumor T_{RM} and non-T_{RM} (n = 10), and in Th17$^+$ control cells (n = 2).

(G) Expression of pSTAT3 (gMFI) in tumor T_{RM} and non-T_{RM} cells (n = 10), and in Th17$^+$ controls (n = 2). Right, expression of pSTAT3 (gMFI) in tumor T_{RM} cells displaying CD103^{high} (High), CD103^{int} (Int), and CD103^{low} (Low) phenotype, and in CD103$^-$CD8$^+$ TILs (Neg) (n = 10).

Each symbol represents an individual donor; horizontal lines are means ± SEM. *$p < 0.05$, **$p < 0.01$, and ***$p < 0.001$ (paired t test or ANOVA with Bonferroni post hoc test). gMFI, geometric mean fluorescence intensity; ns: not significant.

See also Figure S5 and Tables S8 and S9

CellPress
OPEN ACCESS

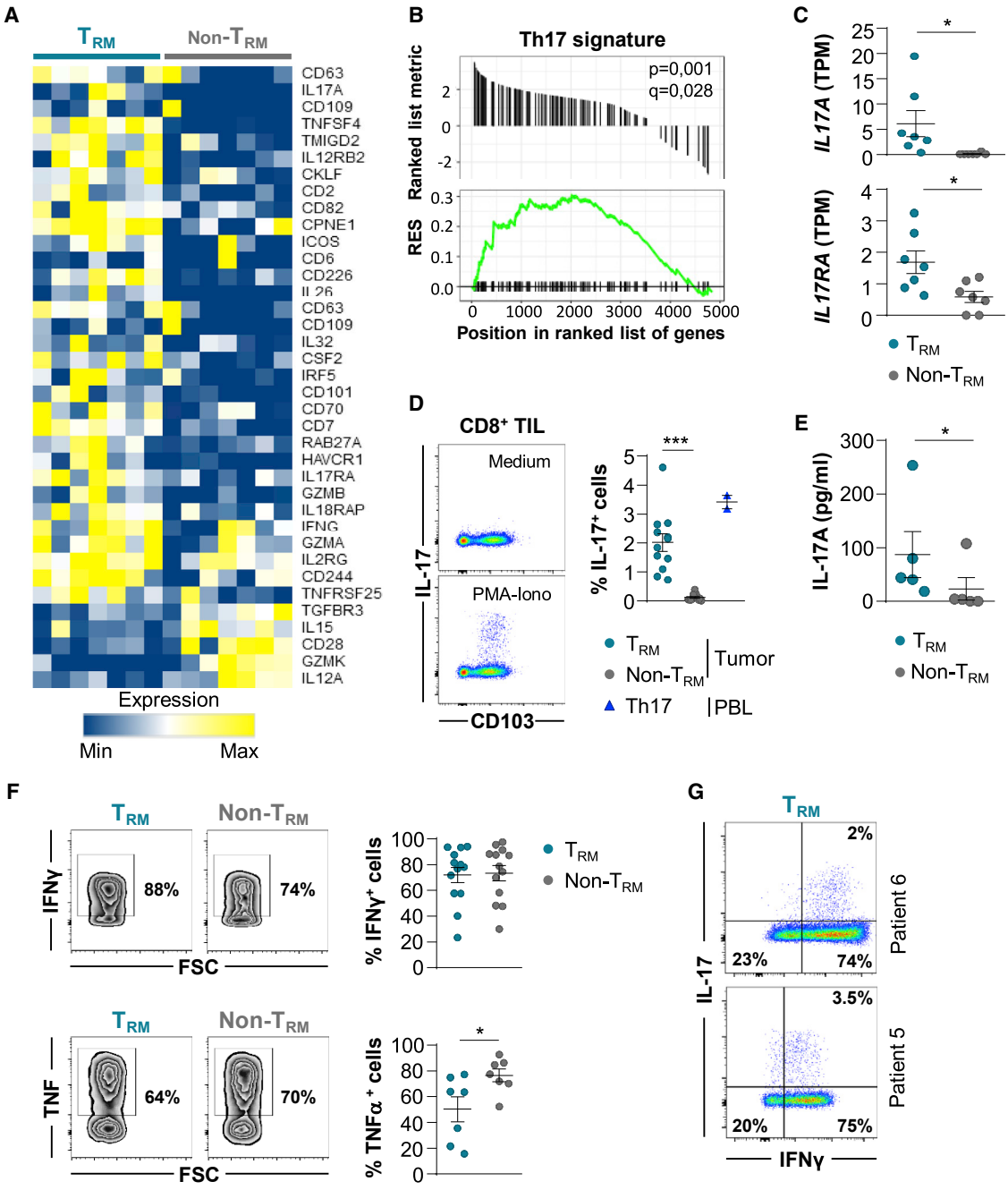

Figure 5. A Subset of Tumor CD103$^+$CD8$^+$ T_{RM} Cells Displays a Tc17-Polarized Pattern

(A) Heatmap of activation gene signature differentially expressed in paired CD103$^+$ and KLRG1$^+$ CD8$^+$ TIL (n = 7) ($p < 0.05$).

(B) GSEA of gene set from the Th17 signature in the transcriptome of CD103$^+$CD8$^+$ TILs relative to KLRG1$^+$CD8$^+$ TILs (n = 7). Running enrichment score (RES) for the gene set as the analysis "walks down" the ranked list of genes; the position of gene set members (black vertical lines) in the ranked list of genes and the value of ranking metric are shown.

(C) Expression of *IL17A* and *IL17RA* transcripts encoding IL-17 and IL-17R, respectively, in tumor T_{RM} and non-T_{RM} cells (n = 7). TPMs are shown.

(D) Intracellular expression of IL-17 in CD8$^+$ TILs stimulated for 4 h with PMA plus ionomycin. One representative dot plot is shown. Right, percentages of IL-17$^+$ cells among T_{RM} and non-T_{RM} cells from tumors (n = 12). Healthy donor Th17$^+$ control cells are included (n = 2).

(E) Production of IL-17 measured by ELISA in supernatant of tumor T_{RM} and non-T_{RM} cells stimulated overnight with PMA plus ionomycin. The data are concentrations of IL-17 in picograms per milliliter per 100,000 cells (n = 5).

(F) Intracellular expression of IFN-γ and TNF-α in CD8$^+$ TILs stimulated with PMA plus ionomycin. The dot plots from 1 representative patient are shown. Right, percentages of IFN-γ$^+$ (n = 13) and TNF-α$^+$ (n = 7) cells among T_{RM} and non-T_{RM} cells from tumors.

(legend continued on next page)

expressed in human NSCLC CD103$^+$CD8$^+$ T_{RM} cells, and this expression is likely induced by TGF-β at the tumor site. In this regard, Zeb1 has emerged as a critical transcription factor for memory T cell survival and function.[30] At least a subset of NSCLC CD8$^+$ T_{RM} cells displays a transcription factor profile characteristic of Th17/Tc17 lymphocytes, with expression of Aiolos, pSTAT3, and AhR. The upregulation of Aiolos by STAT3 and AhR was reported to promote Th17 differentiation by silencing IL-2 expression.[31] In contrast, *TCF7*/TCF-1 was less abundant in NSCLC T_{RM}s than in non-T_{RM} cells. The downregulation of *TCF7*/TCF-1 in CD103$^+$CD8$^+$ TILs is consistent with previous single-cell analyses of T_{RM} cells from breast cancer and NSCLC.[7,8] Exhausted PD1$^+$CD8$^+$ TILs from human melanoma are also *TCF7*^{neg} and enriched with CD39- and CD103-expressing cells.[20,32] Notably, the activation of TCR leads to the downregulation of TCF-1 in human CD8$^+$ T cells,[33] suggesting recent TCR engagement of TCF-1^{low} NSCLC T_{RM} cells. These TCF-1$^{low/neg}$ CD8$^+$ cells, as opposed to bystander TCF-1$^+$ TILs, are tumor-reactive CTLs,[8,20,32,34] highlighting their anti-tumor potential and suggesting that TCF-1-expressing (stem-like or memory precursor-like) cells are not the only source of T cell expansion following ICB,[35–40] and that TCF-1^{low} (T_{RM}) cells are also reactivated to participate in the response to anti-PD-1.

TCF7 emerges as a central transcription factor in CD8$^+$ T_{RM} differentiation in IL-17-producing lymphocytes, as its downregulation results in enhanced Tc17-cell development.[41] Consistently, our functional experiments showed that a small subset of NSCLC CD8$^+$ T_{RM} cells produces IL-17 after PMA/ionomycin stimulation at frequencies similar to heathy donor Th17/Tc17-polarized T cells. Human CD8$^+$CD49a$^-$ T_{RM} cells were also found to produce IL-17 in skin epithelia and psoriasis lesions, promoting local inflammation.[42] Differentiation of a subpopulation of CD8$^+$ T_{RM} cells into the Tc17 lineage is likely associated with the secretion of IL-6 and TGF-β by lung tumor cells themselves and the inhibition of IFNγ, conditions known to promote the formation of murine CD4$^+$ Th17 lineage.[43] Murine Tc17/IFNγ CD8$^+$ T cells mediate improved the anti-tumor immunity that is associated with enhanced survival.[44] A small subset of NSCLC CD103$^+$CD8$^+$ T_{RM} cells also produces IL-17 and IFN-γ, displays increased proliferative potential, and mediates cytotoxic function toward autologous cancer cells correlated with the production of granzyme B and the formation of stable conjugates with the cognate target.

The notion that CD103 is a marker of antigen-specific T cells is supported by studies of antiviral and anti-tumor CTL responses, demonstrating that the integrin is induced on CD8$^+$ T cells specific to influenza virus in the lung,[45] Epstein-Barr virus (EBV) in the tonsil,[46] cancer testis antigen NY-ESO-1 in ovarian cancer,[47] and the α-actinin 4 (actn-4) neoepitope in NSCLC.[48] The tumor antigen specificity of CD103$^+$CD8$^+$ T_{RM} cells was further emphasized by TCR-seq analyses revealing the expansion of particular TCR clonotypes in CD103$^+$CD8$^+$ TILs, but to a lesser extent in KLRG1$^+$CD8$^+$ TILs. TCR clonality in tumor CD8$^+$ T_{RM} cells correlated with high PD-1 expression, which reflects their strong activation state and suggests high TCR avidity for the tumor antigen, resulting in antigen-driving T cell proliferation. Remarkably, CD103$^+$CD8$^+$ T_{RM} cells were shown to expand during anti-PD-1 immunotherapy of melanoma[49] and lung carcinoma patients.[8] Here, we provide evidence that a high density of CD103$^+$CD8$^+$ T_{RM} cells in tumors was associated with greatly improved PFS in NSCLC patients treated with anti-PD-(L)1 as a single agent. We also provide evidence that the density of CD103$^+$CD8$^+$ TIL was increased in tumors after anti-PD-1 treatment, suggesting that PD-1 blockade reactivates this tumor-specific T_{RM} subset, which proliferates and exerts cytotoxic activity so as to participate in anti-tumor immunity and response to ICB. The reason for intertumor T_{RM} density variation is not understood, but it may reflect interpatient variations in the number of antigen-specific T cell precursors, the tumor mutational burden, or the amount of active TGF-β required for CD103 expression in TCR-engaged T lymphocytes.[16,48,50] In regard to epithelial tumor regions, enhanced infiltration by CD103$^+$CD8$^+$ T_{RM} cells did not correlate with E-cadherin expression levels by cancer cells. Consistent results were obtained in ovarian cancer,[3] but not in bladder cancer, where intratumoral infiltration of CD103$^+$ TIL was associated with the expression of E-cadherin on tumor cells.[51] Although the enhanced expression of ICAM-1 on cancer cells was not associated with the increased density of CD103$^+$CD8$^+$ TIL in epithelial tumor islets, the combination with high T_{RM} infiltration improved patient PFS. This may be associated with strong adhesion between tumor cells and specific T_{RM} cells provided by the ICAM-1-LFA-1 interaction and required for effective target cell lysis by activated CTLs.[17,52] In contrast, the infiltration of epithelial tumor regions by CD103$^-$CD8$^+$ TIL did not result in the improved survival of anti-PD-1-treated patients. This is surprising, since previous studies reported that CD8$^+$ T cell infiltration is associated with better clinical outcomes and response to ICB.[1] Although the status of CD8$^+$ TILs for CD103 expression was not investigated, these T cells likely expressed the integrin, since it is required for their recruitment and functionality within epithelial tumor regions.[53]

Overall, our study demonstrates a major role for CD103$^+$CD8$^+$ T_{RM} cells in anti-tumor immunity and the response to anti-PD-1 in lung cancer. It also delineates CD103 as a biomarker that is able to accurately identify the repertoire of clonally expanded tumor-reactive CD8$^+$ T cells. These CD103$^+$ CD8$^+$ T cells are activated, proliferate, a subset of which can produce IL-17 and IFNγ, and effectively kill autologous malignant cells. Thus, investigating CD103$^+$CD8$^+$ T_{RM} cells in cancer patients not only contributes to our understanding of the local anti-tumor CTL response but it also provides insight into the role of this T cell population in response to ICB. Improved responses to anti-PD-1 in patients with high

(G) Intracellular co-expression of IL-17 and IFN-γ in tumor T_{RM} cells stimulated with PMA plus ionomycin. Two representative patients are shown.
Symbols represent individual TILs or lung samples; horizontal lines are means ± SEMs (C, D, E, and F). *$p < 0.05$ and *** $p < 0.001$ (paired t test or ANOVA with Bonferroni post hoc test).
See also Figure S5 and Table S8.

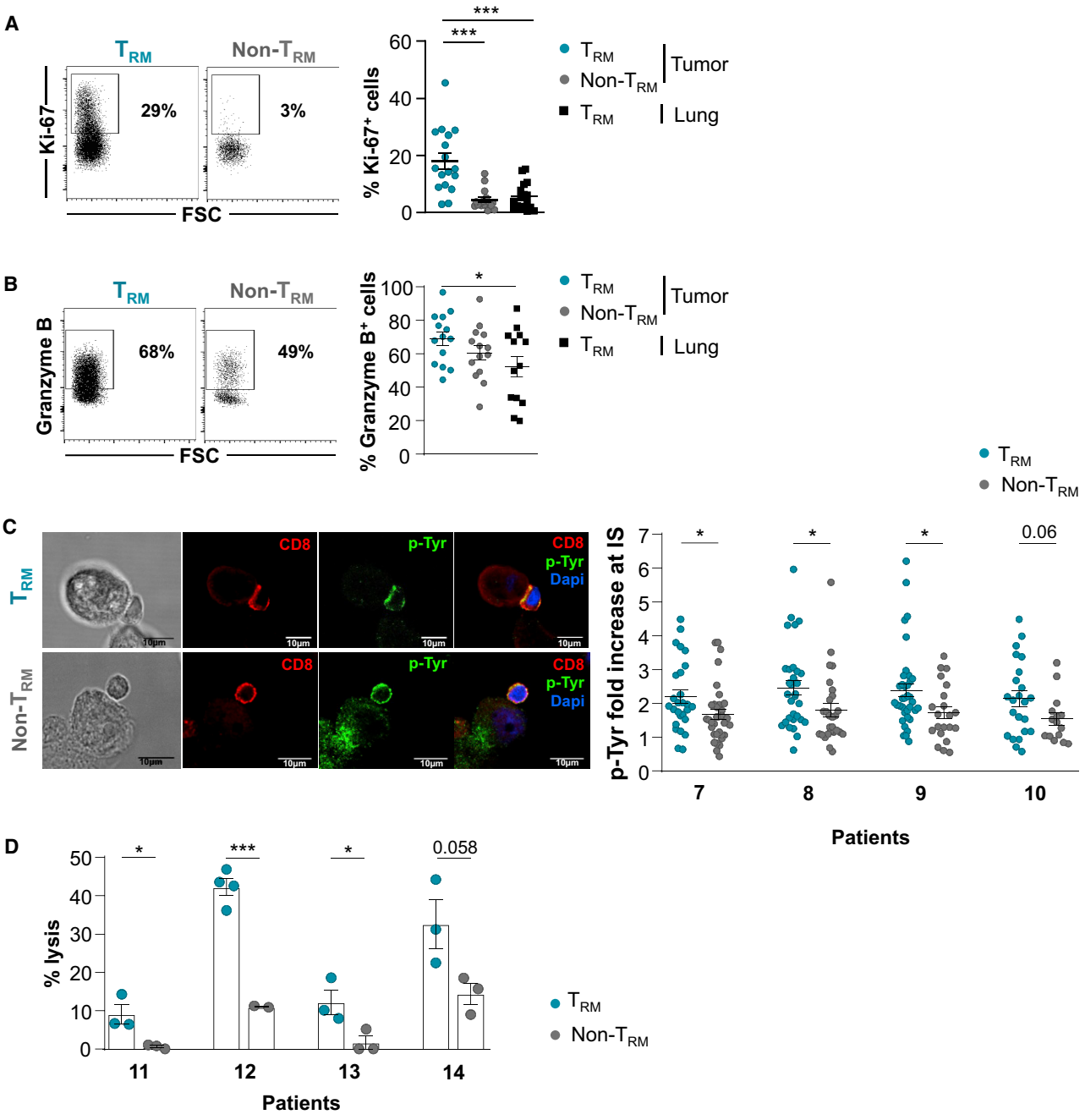

Figure 6. T_{RM} Cells Are Tumor-Specific $CD8^+$ T Cells

(A) Intracellular expression of Ki67 in T_{RM} and non-T_{RM} cells from NSCLCs. The dot plot of 1 representative patient is shown. Right, percentages of $Ki67^+$ cells in paired T_{RM} and non-T_{RM} cells from tumors and paired T_{RM} cells from healthy lung (n = 18).

(B) Intracellular expression of granzyme B in tumor T_{RM} and non-T_{RM} cells. The dot plot of 1 representative patient is shown. Right, percentages of granzyme B^+ cells in T_{RM} and non-T_{RM} cells from tumors and paired T_{RM} cells from healthy lung (n = 14).

(C) Conjugates formed between freshly isolated $CD8^+$ tumor T_{RM} or non-T_{RM} cells and autologous tumor cells were analyzed by confocal microscopy for p-Tyr (green fluorescence) accumulation in the contact area. T cells were labeled with anti-CD8 mAb (red). Scale bars, 10 μm. Right, quantification of pTyr fluorescence intensity fold increase in CD8 T cells at contact zone with cognate target cells. Four representative patients are included. Each symbol represents an individual synapse from 15 to 37 analyzed conjugates.

(D) Cytotoxic activity of freshly isolated tumor T_{RM} and non-T_{RM} cells toward autologous cancer cells determined by a conventional 4 h chromium release assay at a 20:1 E:T ratio. The data correspond to 4 independent experiments with 4 different tumor samples. Horizontal lines are means ± SEMs from triplicate.

Symbols represent individual TILs or lung samples; horizontal lines are means ± SEMs (A and B). *$p < 0.05$ and ***$p < 0.001$ (paired t test or ANOVA with Bonferroni post hoc test).

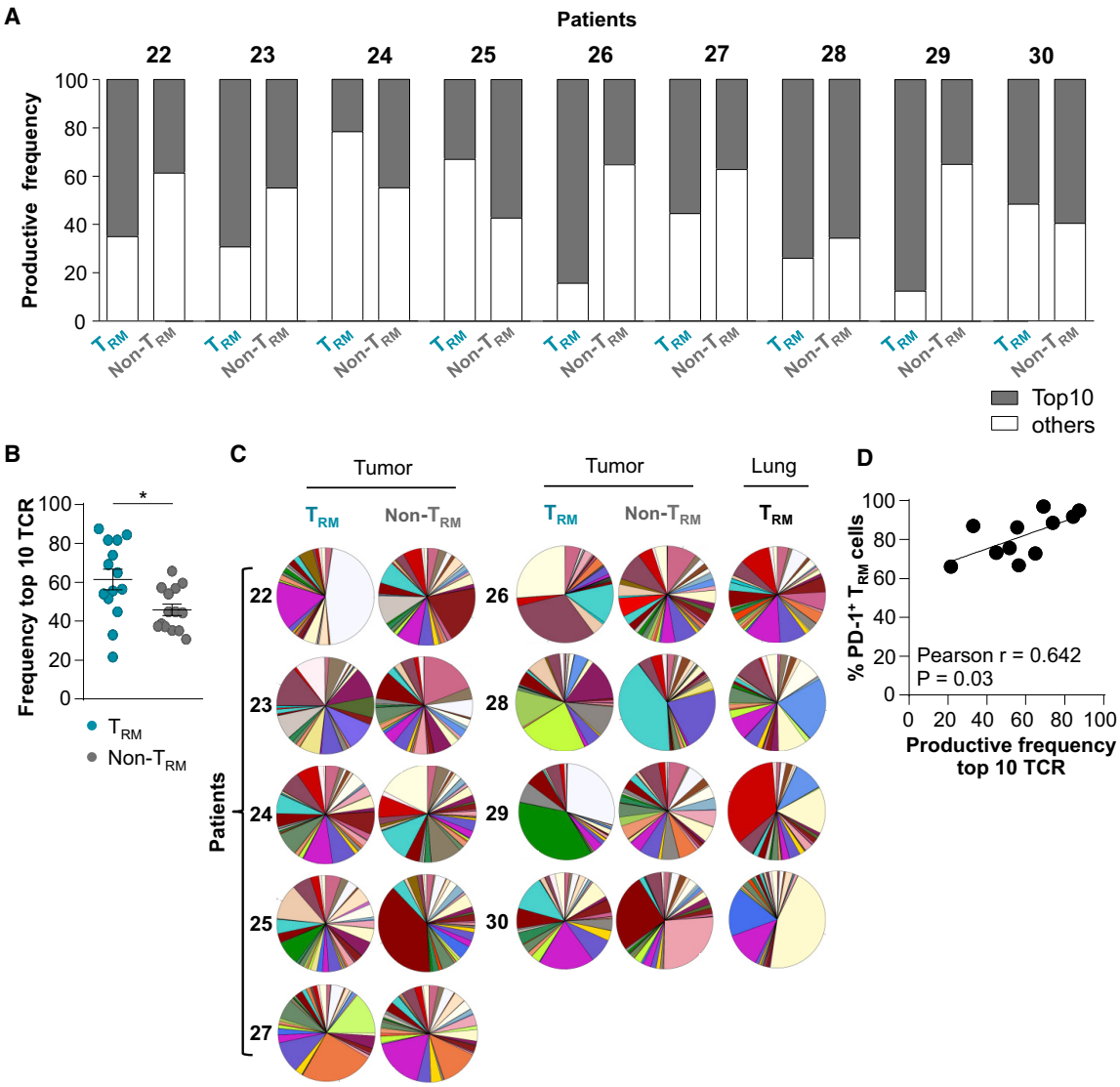

Figure 7. Tumor CD8$^+$ T_{RM} Cells Display an Oligoclonal TCR Repertoire

(A) Frequency of productive TCR sequences of the top 10 clonotypes (gray) and all other clonotypes (white) in paired NSCLC T_{RM} and non-T_{RM} cells from each patient sample (patients 22–30). TCR-β CDR3 region in tumor T_{RM} and non-T_{RM} cells were analyzed by TCR-seq (n = 9).

(B) Frequency of the top 10 TCR sequences in tumor T_{RM} and non-T_{RM} cells from both TCR-seq and RNA-seq (n = 14).

(C) Pie charts illustrating distribution of TCRV-β families in T_{RM} and non-T_{RM} cells from tumors (n = 9) and autologous T_{RM} cells from healthy lungs (n = 4).

(D) Correlation between productive frequency of the top 10 TCR clonotypes and the percentage of PD-1$^+$ cells in tumor T_{RM}s (n = 11).

Horizontal lines correspond to means ± SEMs.

*$p < 0.05$ paired t test; ns, not significant. The r value indicates the Pearson correlation coefficient.

See also Figure S6.

densities of tumor CD103$^+$CD8$^+$ T_{RM} cells, even after having undergone resection of their tumor, may be associated with a pool of cancer-specific CD8$^+$ T cells present in bone marrow, as has been described in infectious diseases.[54] This non-circulating memory CD8$^+$ T cell subset develops in response to a wide variety of antigens, including tumor antigens, and expands upon antigen rechallenge. Thus, CD103$^+$CD8$^+$ T_{RM} cells appear to be crucial components in immune protection against cancer and in the response of NSCLC to ICB, opening up new avenues in cancer immunotherapy.

Limitations of Study

The total CD8^{+high} population in the stroma was as correlative as the CD103$^+$CD8^{+high} population (both with 30.62 months of PFS), most likely due to the frequent expression of CD103 on CD8$^+$ TILs even in the stroma. The study lacks functional features on IL-17-producing T_{RM} cells. Isolation from the same tumor of IL-17$^+$ and IL-17$^-$ CD8$^+$CD103$^+$ TILs and sufficient numbers of autologous tumor cells will help to further characterize this small T_{RM} cell subset. Single-cell RNA-seq of the tumor T_{RM} population may help define the molecular

features of Tc17 cells. TCR-γδ lymphocytes may contribute to IL-17 production in the TME, even though their total number is very weak.

STAR★METHODS

Detailed methods are provided in the online version of this paper and include the following:

- KEY RESOURCES TABLE
- RESOURCE AVAILABILITY
  - Lead Contact
  - Materials Availability
  - Data and Code Availability
- EXPERIMENTAL MODEL AND SUBJECT DETAILS
  - Patient cohort characteristics and tumor samples
- METHOD DETAILS
  - Immunohistochemical staining
  - Tumor cells and tissue-infiltrating lymphocytes isolation
  - RNA and TCR sequencing and analyses
  - Flow cytometry and ELISA
  - Conjugate formation and cytotoxic experiments
- QUANTIFICATION AND STATISTICAL ANALYSIS

SUPPLEMENTAL INFORMATION

Supplemental Information can be found online at https://doi.org/10.1016/j.xcrm.2020.100127.

ACKNOWLEDGMENTS

This work was supported by grants from the Institut National du Cancer (INCa; PLBIO016-080 grant no. 10557); the "Association pour la Recherche sur le Cancer (ARC; grant nos. PJA20161204720, SIGN'IT20181007792, and PJA20181208049), Ligue Contre le Cancer (Comité des Yvelines, grant no. 9FI12414QLCZ and Comité du Val de Marne, 2019) and Bristol-Myers Squibb (BMS, France; grant no. CA209-942). S. Corgnac was supported by a grant from the Groupement des Entreprises Françaises dans la Lutte Contre le Cancer (GEFLUC; grant no. 2016-R16180LL) and Cancéropôle Ile de France, and was a recipient of a fellowship from Fondation Recherche Medicale (FRM), Gustave Roussy (SIRIC-SOCRATE), and INCa (PLBIO016-080 grant no. 10557). I.M. was the recipient of a fellowship from the Ligue National Contre le Cancer. M.L. was a recipient of a MENRT fellowship from the French Ministry of Research, a fellowship from the Ligue Contre le Cancer and Gustave Roussy (SIRIC-SOCRATE), and a Taxe d'apprentissage TA-2016 from École des Sciences du Cancer de Gustave Roussy/Université Paris-Sud. We thank Georges Bismuth from Cochin Hospital and Eric Tartour from Hôpital Européen Georges Pompidou for critically reading this manuscript. We also thank Yann Lecluse, Cyril Catelain and Philippe Rameau from the cytometry facility (Plateforme d'Imagerie-Cytométrie), Virginie Marty from the platform of histocytopathology (Centre de Ressources Biologiques [CRB]), and Yahia Adnani, Aziza Caidi, Guillaume Meurice and Marc Deloger from the platform of bioinformatics (INSERM US23, CNRS UMS3655) of Gustave Roussy for their help with flow cytometry, lung tumor specimens, and RNA-seq analyses and data file deposit, respectively. We are grateful to José-Carlos Benitez-Montanez, Jihène Lahmar-Bach-Hamba, Jordi Remon-Masip, Maud Ngocamus, and Claudio Nicotra from the Department of Cancer Medicine of Gustave Roussy for their help in establishing patient tumor cohorts. We also thank Vassili Soumelis from Institut Curie for help with the RNA extraction protocol and Caroline Communaux from the CRB of Marie Lannelongue Hospital for help with fresh human NSCLC tumors. The graphical abstract was created with BioRender.

AUTHOR CONTRIBUTIONS

Conception and design, S. Corgnac. and F.M.-C. Development of Methodology, S. Corgnac, I.M., N.D., J.A., and F.M.-C. Data Acquisition (e.g., providing animals, acquiring and managing patients, providing facilities), S. Corgnac, I.M., L.M., E.A., H.H., T.D., M.L., E.V., J.K., L.G., N.S., P.V., V.d.M., O.M., J.-Y.S., C.M., S. Chouaib, D.P., J.A., B.B., and F.M.-C. Data Analysis & Interpretation (e.g., statistical analysis, biostatistics, computational analysis), S. Corgnac, E.A., L.M., J.A., B.B., and F.M.-C. Writing, Reviewing, and/or Revision of Manuscript, S. Corgnac and F.M.-C. Administrative, Technical, and Material Support (e.g., reporting and organizing data, constructing databases), S. Corgnac, I.M., L.M., E.A., P.V., V.d.M., O.M., J.-Y.S., C.M., B.B., and F.M.-C. Study Supervision, F.M.-C.

DECLARATION OF INTERESTS

B.B.'s sponsored research at Gustave Roussy Cancer Center consists of the following: Abbvie, Amgen, AstraZeneca, BeiGene, Blueprint Medicines, BMS, Boehringer Ingelheim, Celgene, Cristal Therapeutics, Daiichi-Sankyo, Eli Lilly, GSK, Ignyta, IPSEN, Inivata, Janssen, Merck KGaA, MSD, Nektar, Onxeo, OSE Immunotherapeutics, Pfizer, Pharma Mar, Roche-Genentech, Sanofi, Servier, Spectrum Pharmaceuticals, Takeda, Tiziana Pharma, and Tolero Pharmaceuticals.

Received: August 22, 2019
Revised: July 24, 2020
Accepted: September 24, 2020
Published: October 20, 2020

REFERENCES

1. Tumeh, P.C., Harview, C.L., Yearley, J.H., Shintaku, I.P., Taylor, E.J., Robert, L., Chmielowski, B., Spasic, M., Henry, G., Ciobanu, V., et al. (2014). PD-1 blockade induces responses by inhibiting adaptive immune resistance. Nature *515*, 568–571.
2. McGranahan, N., Furness, A.J., Rosenthal, R., Ramskov, S., Lyngaa, R., Saini, S.K., Jamal-Hanjani, M., Wilson, G.A., Birkbak, N.J., Hiley, C.T., et al. (2016). Clonal neoantigens elicit T cell immunoreactivity and sensitivity to immune checkpoint blockade. Science *351*, 1463–1469.
3. Webb, J.R., Milne, K., Watson, P., Deleeuw, R.J., and Nelson, B.H. (2014). Tumor-infiltrating lymphocytes expressing the tissue resident memory marker CD103 are associated with increased survival in high-grade serous ovarian cancer. Clin. Cancer Res. *20*, 434–444.
4. Djenidi, F., Adam, J., Goubar, A., Durgeau, A., Meurice, G., de Montpréville, V., Validire, P., Besse, B., and Mami-Chouaib, F. (2015). CD8+CD103+ tumor-infiltrating lymphocytes are tumor-specific tissue-resident memory T cells and a prognostic factor for survival in lung cancer patients. J. Immunol. *194*, 3475–3486.
5. Ganesan, A.P., Clarke, J., Wood, O., Garrido-Martin, E.M., Chee, S.J., Mellows, T., Samaniego-Castruita, D., Singh, D., Seumois, G., Alzetani, A., et al. (2017). Tissue-resident memory features are linked to the magnitude of cytotoxic T cell responses in human lung cancer. Nat. Immunol. *18*, 940–950.
6. Nizard, M., Roussel, H., Diniz, M.O., Karaki, S., Tran, T., Voron, T., Dransart, E., Sandoval, F., Riquet, M., Rance, B., et al. (2017). Induction of resident memory T cells enhances the efficacy of cancer vaccine. Nat. Commun. *8*, 15221.
7. Savas, P., Virassamy, B., Ye, C., Salim, A., Mintoff, C.P., Caramia, F., Salgado, R., Byrne, D.J., Teo, Z.L., Dushyanthen, S., et al.; Kathleen Cuningham Foundation Consortium for Research into Familial Breast Cancer (kConFab) (2018). Single-cell profiling of breast cancer T cells reveals a tissue-resident memory subset associated with improved prognosis. Nat. Med. *24*, 986–993.
8. Clarke, J., Panwar, B., Madrigal, A., Singh, D., Gujar, R., Wood, O., Chee, S.J., Eschweiler, S., King, E.V., Awad, A.S., et al. (2019). Single-cell

transcriptomic analysis of tissue-resident memory T cells in human lung cancer. J. Exp. Med. *216*, 2128–2149.

9. Mackay, L.K., Stock, A.T., Ma, J.Z., Jones, C.M., Kent, S.J., Mueller, S.N., Heath, W.R., Carbone, F.R., and Gebhardt, T. (2012). Long-lived epithelial immunity by tissue-resident memory T (TRM) cells in the absence of persisting local antigen presentation. Proc. Natl. Acad. Sci. USA *109*, 7037–7042.
10. Hofmann, M., and Pircher, H. (2011). E-cadherin promotes accumulation of a unique memory CD8 T-cell population in murine salivary glands. Proc. Natl. Acad. Sci. USA *108*, 16741–16746.
11. Ray, S.J., Franki, S.N., Pierce, R.H., Dimitrova, S., Kotliansky, V., Sprague, A.G., Doherty, P.C., de Fougerolles, A.R., and Topham, D.J. (2004). The collagen binding alpha1beta1 integrin VLA-1 regulates CD8 T cell-mediated immune protection against heterologous influenza infection. Immunity *20*, 167–179.
12. McNamara, H.A., Cai, Y., Wagle, M.V., Sontani, Y., Roots, C.M., Miosge, L.A., O'Connor, J.H., Sutton, H.J., Ganusov, V.V., Heath, W.R., et al. (2017). Up-regulation of LFA-1 allows liver-resident memory T cells to patrol and remain in the hepatic sinusoids. Sci. Immunol. *2*, eaaj1996.
13. Mackay, L.K., Minnich, M., Kragten, N.A., Liao, Y., Nota, B., Seillet, C., Zaid, A., Man, K., Preston, S., Freestone, D., et al. (2016). Hobit and Blimp1 instruct a universal transcriptional program of tissue residency in lymphocytes. Science *352*, 459–463.
14. Hombrink, P., Helbig, C., Backer, R.A., Piet, B., Oja, A.E., Stark, R., Brasser, G., Jongejan, A., Jonkers, R.E., Nota, B., et al. (2016). Programs for the persistence, vigilance and control of human CD8$^+$ lung-resident memory T cells. Nat. Immunol. *17*, 1467–1478.
15. Milner, J.J., Toma, C., Yu, B., Zhang, K., Omilusik, K., Phan, A.T., Wang, D., Getzler, A.J., Nguyen, T., Crotty, S., et al. (2017). Runx3 programs CD8$^+$ T cell residency in non-lymphoid tissues and tumours. Nature *552*, 253–257.
16. Le Floc'h, A., Jalil, A., Vergnon, I., Le Maux Chansac, B., Lazar, V., Bismuth, G., Chouaib, S., and Mami-Chouaib, F. (2007). Alpha E beta 7 integrin interaction with E-cadherin promotes antitumor CTL activity by triggering lytic granule polarization and exocytosis. J. Exp. Med. *204*, 559–570.
17. Anikeeva, N., Somersalo, K., Sims, T.N., Thomas, V.K., Dustin, M.L., and Sykulev, Y. (2005). Distinct role of lymphocyte function-associated antigen-1 in mediating effective cytolytic activity by cytotoxic T lymphocytes. Proc. Natl. Acad. Sci. USA *102*, 6437–6442.
18. Johnston, R.J., Comps-Agrar, L., Hackney, J., Yu, X., Huseni, M., Yang, Y., Park, S., Javinal, V., Chiu, H., Irving, B., et al. (2014). The immunoreceptor TIGIT regulates antitumor and antiviral CD8(+) T cell effector function. Cancer Cell *26*, 923–937.
19. Guo, X., Zhang, Y., Zheng, L., Zheng, C., Song, J., Zhang, Q., Kang, B., Liu, Z., Jin, L., Xing, R., et al. (2018). Global characterization of T cells in non-small-cell lung cancer by single-cell sequencing. Nat. Med. *24*, 978–985.
20. Duhen, T., Duhen, R., Montler, R., Moses, J., Moudgil, T., de Miranda, N.F., Goodall, C.P., Blair, T.C., Fox, B.A., McDermott, J.E., et al. (2018). Co-expression of CD39 and CD103 identifies tumor-reactive CD8 T cells in human solid tumors. Nat. Commun. *9*, 2724.
21. Parkhurst, M., Gros, A., Pasetto, A., Prickett, T., Crystal, J.S., Robbins, P., and Rosenberg, S.A. (2017). Isolation of T-Cell Receptors Specifically Reactive with Mutated Tumor-Associated Antigens from Tumor-Infiltrating Lymphocytes Based on CD137 Expression. Clin. Cancer Res. *23*, 2491–2505.
22. Gros, A., Robbins, P.F., Yao, X., Li, Y.F., Turcotte, S., Tran, E., Wunderlich, J.R., Mixon, A., Farid, S., Dudley, M.E., et al. (2014). PD-1 identifies the patient-specific CD8$^+$ tumor-reactive repertoire infiltrating human tumors. J. Clin. Invest. *124*, 2246–2259.
23. Takada, K., Wang, X., Hart, G.T., Odumade, O.A., Weinreich, M.A., Hogquist, K.A., and Jameson, S.C. (2011). Kruppel-like factor 2 is required for trafficking but not quiescence in postactivated T cells. J. Immunol. *186*, 775–783.
24. Skon, C.N., Lee, J.Y., Anderson, K.G., Masopust, D., Hogquist, K.A., and Jameson, S.C. (2013). Transcriptional downregulation of S1pr1 is required for the establishment of resident memory CD8+ T cells. Nat. Immunol. *14*, 1285–1293.
25. Cepek, K.L., Shaw, S.K., Parker, C.M., Russell, G.J., Morrow, J.S., Rimm, D.L., and Brenner, M.B. (1994). Adhesion between epithelial cells and T lymphocytes mediated by E-cadherin and the alpha E beta 7 integrin. Nature *372*, 190–193.
26. Shiow, L.R., Rosen, D.B., Brdicková, N., Xu, Y., An, J., Lanier, L.L., Cyster, J.G., and Matloubian, M. (2006). CD69 acts downstream of interferon-alpha/beta to inhibit S1P1 and lymphocyte egress from lymphoid organs. Nature *440*, 540–544.
27. Simoni, Y., Becht, E., Fehlings, M., Loh, C.Y., Koo, S.L., Teng, K.W.W., Yeong, J.P.S., Nahar, R., Zhang, T., Kared, H., et al. (2018). Bystander CD8$^+$ T cells are abundant and phenotypically distinct in human tumour infiltrates. Nature *557*, 575–579.
28. Scott, A.C., Dundar, F., Zumbo, P., Chandran, S.S., Klebanoff, C.A., Shakiba, M., Trivedi, P., Menocal, L., Appleby, H., Camara, S.J., et al. (2019). TOX is a critical regulator of tumour-specific T cell differentiation. Nature *571*, 270–274.
29. Mackay, L.K., Braun, A., Macleod, B.L., Collins, N., Tebartz, C., Bedoui, S., Carbone, F.R., and Gebhardt, T. (2015). Cutting edge: CD69 interference with sphingosine-1-phosphate receptor function regulates peripheral T cell retention. J. Immunol. *194*, 2059–2063.
30. Guan, T., Dominguez, C.X., Amezquita, R.A., Laidlaw, B.J., Cheng, J., Henao-Mejia, J., Williams, A., Flavell, R.A., Lu, J., and Kaech, S.M. (2018). ZEB1, ZEB2, and the miR-200 family form a counterregulatory network to regulate CD8$^+$ T cell fates. J. Exp. Med. *215*, 1153–1168.
31. Quintana, F.J., Jin, H., Burns, E.J., Nadeau, M., Yeste, A., Kumar, D., Rangachari, M., Zhu, C., Xiao, S., Seavitt, J., et al. (2012). Aiolos promotes TH17 differentiation by directly silencing Il2 expression. Nat. Immunol. *13*, 770–777.
32. Li, H., van der Leun, A.M., Yofe, I., Lubling, Y., Gelbard-Solodkin, D., van Akkooi, A.C.J., van den Braber, M., Rozeman, E.A., Haanen, J., Blank, C.U., et al. (2019). Dysfunctional CD8 T Cells Form a Proliferative, Dynamically Regulated Compartment within Human Melanoma. Cell *176*, 775–789.e18.
33. Willinger, T., Freeman, T., Herbert, M., Hasegawa, H., McMichael, A.J., and Callan, M.F. (2006). Human naive CD8 T cells down-regulate expression of the WNT pathway transcription factors lymphoid enhancer binding factor 1 and transcription factor 7 (T cell factor-1) following antigen encounter in vitro and in vivo. J. Immunol. *176*, 1439–1446.
34. Brummelman, J., Mazza, E.M.C., Alvisi, G., Colombo, F.S., Grilli, A., Mikulak, J., Mavilio, D., Alloisio, M., Ferrari, F., Lopci, E., et al. (2018). High-dimensional single cell analysis identifies stem-like cytotoxic CD8$^+$ T cells infiltrating human tumors. J. Exp. Med. *215*, 2520–2535.
35. Im, S.J., Hashimoto, M., Gerner, M.Y., Lee, J., Kissick, H.T., Burger, M.C., Shan, Q., Hale, J.S., Lee, J., Nasti, T.H., et al. (2016). Defining CD8+ T cells that provide the proliferative burst after PD-1 therapy. Nature *537*, 417–421.
36. Sade-Feldman, M., Yizhak, K., Bjorgaard, S.L., Ray, J.P., de Boer, C.G., Jenkins, R.W., Lieb, D.J., Chen, J.H., Frederick, D.T., Barzily-Rokni, M., et al. (2018). Defining T Cell States Associated with Response to Checkpoint Immunotherapy in Melanoma. Cell *175*, 998–1013.e20.
37. Kurtulus, S., Madi, A., Escobar, G., Klapholz, M., Nyman, J., Christian, E., Pawlak, M., Dionne, D., Xia, J., Rozenblatt-Rosen, O., et al. (2019). Checkpoint Blockade Immunotherapy Induces Dynamic Changes in PD-1(-) CD8(+) Tumor-Infiltrating T Cells. Immunity *50*, 181–194.e6.
38. Miller, B.C., Sen, D.R., Al Abosy, R., Bi, K., Virkud, Y.V., LaFleur, M.W., Yates, K.B., Lako, A., Felt, K., Naik, G.S., et al. (2019). Subsets of

exhausted CD8+ T cells differentially mediate tumor control and respond to checkpoint blockade. Nat. Immunol. *20*, 326–336.

39. Siddiqui, I., Schaeuble, K., Chennupati, V., Fuertes Marraco, S.A., Calderon-Copete, S., Pais Ferreira, D., Carmona, S.J., Scarpellino, L., Gfeller, D., Pradervand, S., et al. (2019). Intratumoral Tcf1(+)PD-1(+)CD8(+) T Cells with Stem-like Properties Promote Tumor Control in Response to Vaccination and Checkpoint Blockade Immunotherapy. Immunity *50*, 195–211.e10.
40. Yost, K.E., Satpathy, A.T., Wells, D.K., Qi, Y., Wang, C., Kageyama, R., McNamara, K.L., Granja, J.M., Sarin, K.Y., Brown, R.A., et al. (2019). Clonal replacement of tumor-specific T cells following PD-1 blockade. Nat. Med. *25*, 1251–1259.
41. Mielke, L.A., Liao, Y., Clemens, E.B., Firth, M.A., Duckworth, B., Huang, Q., Almeida, F.F., Chopin, M., Koay, H.F., Bell, C.A., et al. (2019). TCF-1 limits the formation of Tc17 cells via repression of the MAF-RORγt axis. J. Exp. Med. *216*, 1682–1699.
42. Cheuk, S., Schlums, H., Gallais Sérézal, I., Martini, E., Chiang, S.C., Marquardt, N., Gibbs, A., Detlofsson, E., Introini, A., Forkel, M., et al. (2017). CD49a Expression Defines Tissue-Resident CD8+ T Cells Poised for Cytotoxic Function in Human Skin. Immunity *46*, 287–300.
43. Ichiyama, K., Sekiya, T., Inoue, N., Tamiya, T., Kashiwagi, I., Kimura, A., Morita, R., Muto, G., Shichita, T., Takahashi, R., and Yoshimura, A. (2011). Transcription factor Smad-independent T helper 17 cell induction by transforming-growth factor-β is mediated by suppression of eomesodermin. Immunity *34*, 741–754.
44. Tajima, M., Wakita, D., Satoh, T., Kitamura, H., and Nishimura, T. (2011). IL-17/IFN-γ double producing CD8+ T (Tc17/IFN-γ) cells: a novel cytotoxic T-cell subset converted from Tc17 cells by IL-12. Int. Immunol. *23*, 751–759.
45. Piet, B., de Bree, G.J., Smids-Dierdorp, B.S., van der Loos, C.M., Remmerswaal, E.B., von der Thüsen, J.H., van Haarst, J.M., Eerenberg, J.P., ten Brinke, A., van der Bij, W., et al. (2011). CD8+ T cells with an intraepithelial phenotype upregulate cytotoxic function upon influenza infection in human lung. J. Clin. Invest. *121*, 2254–2263.
46. Woodberry, T., Suscovich, T.J., Henry, L.M., August, M., Waring, M.T., Kaur, A., Hess, C., Kutok, J.L., Aster, J.C., Wang, F., et al. (2005). Alpha E beta 7 (CD103) expression identifies a highly active, tonsil-resident effector-memory CTL population. J. Immunol. *175*, 4355–4362.
47. Webb, J.R., Wick, D.A., Nielsen, J.S., Tran, E., Milne, K., McMurtrie, E., and Nelson, B.H. (2010). Profound elevation of CD8+ T cells expressing the intraepithelial lymphocyte marker CD103 (alphaE/beta7 Integrin) in high-grade serous ovarian cancer. Gynecol. Oncol. *118*, 228–236.
48. Franciszkiewicz, K., Le Floc'h, A., Jalil, A., Vigant, F., Robert, T., Vergnon, I., Mackiewicz, A., Benihoud, K., Validire, P., Chouaib, S., et al. (2009). Intratumoral induction of CD103 triggers tumor-specific CTL function and CCR5-dependent T-cell retention. Cancer Res. *69*, 6249–6255.
49. Edwards, J., Wilmott, J.S., Madore, J., Gide, T.N., Quek, C., Tasker, A., Ferguson, A., Chen, J., Hewavisenti, R., Hersey, P., et al. (2018). CD103+ Tumor-Resident CD8+ T Cells Are Associated with Improved Survival in Immunotherapy-Naïve Melanoma Patients and Expand Significantly During Anti-PD-1 Treatment. Clin. Cancer Res. *24*, 3036–3045.
50. El-Asady, R., Yuan, R., Liu, K., Wang, D., Gress, R.E., Lucas, P.J., Drachenberg, C.B., and Hadley, G.A. (2005). TGF-beta-dependent CD103 expression by CD8(+) T cells promotes selective destruction of the host intestinal epithelium during graft-versus-host disease. J. Exp. Med. *201*, 1647–1657.
51. Wang, B., Wu, S., Zeng, H., Liu, Z., Dong, W., He, W., Chen, X., Dong, X., Zheng, L., Lin, T., and Huang, J. (2015). CD103+ Tumor Infiltrating Lymphocytes Predict a Favorable Prognosis in Urothelial Cell Carcinoma of the Bladder. J. Urol. *194*, 556–562.
52. Franciszkiewicz, K., Le Floc'h, A., Boutet, M., Vergnon, I., Schmitt, A., and Mami-Chouaib, F. (2013). CD103 or LFA-1 engagement at the immune synapse between cytotoxic T cells and tumor cells promotes maturation and regulates T-cell effector functions. Cancer Res. *73*, 617–628.
53. Boutet, M., Gauthier, L., Leclerc, M., Gros, G., de Montpreville, V., Théret, N., Donnadieu, E., and Mami-Chouaib, F. (2016). TGFβ Signaling Intersects with CD103 Integrin Signaling to Promote T-Lymphocyte Accumulation and Antitumor Activity in the Lung Tumor Microenvironment. Cancer Res. *76*, 1757–1769.
54. Pascutti, M.F., Geerman, S., Collins, N., Brasser, G., Nota, B., Stark, R., Behr, F., Oja, A., Slot, E., Panagioti, E., et al. (2019). Peripheral and systemic antigens elicit an expandable pool of resident memory CD8(+) T cells in the bone marrow. Eur. J. Immunol. *49*, 853–872.
55. Patro, R., Duggal, G., Love, M.I., Irizarry, R.A., and Kingsford, C. (2017). Salmon provides fast and bias-aware quantification of transcript expression. Nat. Methods *14*, 417–419.
56. Pimentel, H., Bray, N.L., Puente, S., Melsted, P., and Pachter, L. (2017). Differential analysis of RNA-seq incorporating quantification uncertainty. Nat. Methods *14*, 687–690.
57. Yu, G., Wang, L.G., Han, Y., and He, Q.Y. (2012). clusterProfiler: an R package for comparing biological themes among gene clusters. OMICS *16*, 284–287.
58. Bolotin, D.A., Poslavsky, S., Mitrophanov, I., Shugay, M., Mamedov, I.Z., Putintseva, E.V., and Chudakov, D.M. (2015). MiXCR: software for comprehensive adaptive immunity profiling. Nat. Methods *12*, 380–381.
59. Hothorn, T., and Lausen, B. (2003). On the Exact Distribution of Maximally Selected Rank Statistics. Comput. Stat. Data Anal. *43*, 121–137.

STAR★METHODS

KEY RESOURCES TABLE

REAGENT or RESOURCE	SOURCE	IDENTIFIER
Deposit Data		
Raw RNAseq data	This study	EGAS00001004707
Antibodies		
anti-human CD8 Pacific blue (RPA-T8)	BioLegend	Cat# 301023; RRID:AB_493110
anti-human CD103-FITC (Ber-ACT8)	BioLegend	Cat# 350204; RRID:AB_10639865
anti-human KLRG1-PE (13F12F2)	ebioscience	Cat# 12-9488-42; RRID:AB_2572716
anti-human CD3-Alexa700 (UCHT1)	BioLegend	Cat# 300424; RRID:AB_493741
anti-human CD69-APC-Cy7 (FN50)	BioLegend	Cat# 310914; RRID:AB_314849
anti-human granzyme-B-FITC (GB11)	BioLegend	Cat#515403; RRID:AB_2114575
anti-human TNFα-PE/Dazzle594 (Mab11)	BioLegend	Cat# 502945; RRID:AB_2564172
anti-human Aiolos-Alexa488 (16D9C97)	BioLegend	Cat# 371107; RRID:AB_2616975
anti-human Vα7.2-APC-Cy7 (3C10)	BioLegend	Cat# 351713; RRID:AB_2561995
anti-human CD161-Alexa488 (HP-3G10)	BioLegend	Cat# 339923; RRID:AB_2563938
anti-human TCF-1-PE (7F11A10)	BioLegend	Cat#655207; RRID:AB_2728491
anti-human 4-1BB-PE-Dazzle594 (clone 4B4-1)	BioLegend	Cat#309825; RRID:AB_2566259
anti-human TCR$\gamma\delta$-PerCPCy5.5 (B1)	BioLegend	Cat# 331223; RRID:AB_2563012
anti-human CD103-BV711 (Ber-ACT8)	BD Biosciences	Cat# 563162; RRID:AB_2738039
anti-human CD49-PerCPefluor710 (TS2/7)	Thermo Fisher Scientific	Cat# 46-9490-41; RRID:AB_2573890
anti-human S1PR1-efluor660 (SW4GYPP)	Thermo Fisher Scientific	Cat# 50-3639-41; RRID:AB_2574207
anti-human PD-1-PeCyanine7 (eBioJ105)	Thermo Fisher Scientific	Cat# 25-2799-42; RRID:AB_10853804
anti-human AHR-PerCPefluor710 (FF3399)	Thermo Fisher Scientific	Cat# 46-9854-41; RRID:AB_2573905
anti-human Ki67-PerCPefluor710 (20Raj1)	Thermo Fisher Scientific	Cat# 46-5699-41; RRID:AB_10804404
anti-human IFNγ-APC (B27)	BD Biosciences	Cat# 554702; RRID:AB_398580
anti-human Hobit-Alexa647 (Sanquin-Hobit/1)	BD Biosciences	Cat# 566250; RRID:AB_2739629
anti-human CD45RA-APC (T6D11)	Miltenyi Biotec	Cat#130-098-187; RRID:AB_2660978
anti-human pSTAT3pS727-APC (REA324)	Miltenyi Biotec	Cat# 130-105-000; RRID:AB_2653576
anti-human CD39-APC (MZ18-23C8)	Miltenyi Biotec	Cat#130-100-459; RRID:AB_2660867
anti-human IL17A-PeVio770	Miltenyi Biotec	Cat#130-100-327; RRID:AB_2659809
anti-human/mouse Tbet-APC (REA102)	Miltenyi Biotec	Cat# 130-119-821; RRID:AB_2784465
mouse anti-human phospho-tyrosine (PY20)	BD Biosciences	Cat# 610000; RRID:AB_397423
rabbit anti-human CD8	Thermo Fisher Scientific	Cat#PA1-37298; RRID:AB_2075396
Goat anti-mouse IgG AlexaFluor-488	Thermo Fisher Scientific	Cat# A-11001; RRID:AB_2534069
Goat anti-rabbit AlexaFluor-647	Thermo Fisher Scientific	Cat# A-21244; RRID:AB_2535812
anti-human Pan-keratin (clones AE1/AE3)	Agilent	Cat# M3515; RRID:AB_2132885
IHC anti-human CD8 (clone SP16)	Spring Bioscience	Cat#M3164; RRID:AB_1660846
IHC anti-human CD103 (clone EPR4166-2)	Abcam	Cat#ab129202; RRID:AB_11142856
anti-human ICAM-1 (clone N1C2)	GeneTex	Cat#GTX100450; RRID:AB_1950536
anti-human E-cadherin (clone EP6)	BioSB	Cat#BSB5466
LEAF Purified anti-human CD3 antibody (OKT3)	BioLegend	Cat#317304; RRID:AB_571925
Purified anti-human CD28 antibody (CD28.2)	BioLegend	Cat#302901; RRID:AB_314303
Biological Samples		
Resected lung tumors and adjacent healthy lung tissue samples	Institut mutualiste Montsouris and the Hôpital Marie-Lannelongue	See Tables S1 and S4 for details
Human healthy blood	Établissement français du sang, Paris, France	N/A

(*Continued on next page*)

Continued

REAGENT or RESOURCE	SOURCE	IDENTIFIER
Chemicals, Peptides, and Recombinant Proteins		
Phorbol 12-myristate 13-acetate (PMA)	Sigma-Aldrich	Cat#P1585
ionomycine	Sigma-Aldrich	Cat#10634
recombinant IL-2	Sanofi recherche	Cat#1A1
recombinant human TGF-β1	R&D Systems	Cat#240-B-002
recombinant human IL-6	Miltenyi Biotec	Cat# 130-095-365
BrefeldinA	Thermo Fisher Scientific	Cat#00-4506-51
Chromium-51 Radionuclide	Perkin Elmer	Cat#NEZ030005MC
Critical Commercial Assays		
CD8 Microbeads, human	Miltenyi Biotec	Cat#130-045-201
Tumor cells Isolation Kit, human	Miltenyi Biotec	Cat#130-108-339
Human Tumor dissociation kit	Miltenyi Biotec	Cat#130-095-929
Foxp3/Transcription Factor Staining Buffer Set	Thermo Fisher Scientific	Cat#00-5523-00
Single cell RNA purification kit	Norgen	Cat#51800
SureSelect Automated Strand-Specific RNA Library Preparation Kit	Agilent	Cat#G9691A
QIAamp DNA micro kit	QIAGEN	Cat#56304
Maxima first strand cDNA synthesis kit	Thermo-Fischer Scientific	Cat#K1641
Maxima SYBR Green Master Mix	ThermoFischer Scientific	Cat#4472908
LIVE/DEAD Fixable UV dead cell stain kit	ThermoFischer	Cat#L34962
Human IL-17A ELISA Kit	Biotechne	Cat#DY317-05
Opal 7-color Automation IHC Kit	Akoya/Perkin Elmer	NEL801001KT
Oligonucleotides		
Primer sequences for IKZF3, RORC,AHR, IL17A, TCF7, S1PR1 and 18S	This paper; See Table S10	N/A
Software and Algorithms		
GraphPad Prism software V8	GraphPad Software Inc.	RRID:SCR_002798
FlowJo V10	Tree Star Inc	RRID: SCR_008520
RStudio software	The R Foundation	RRID:SCR_000432
InForm software	Akoya/PerkinElmer	N/A
R (v 3.2.3)	The R Foundation	RRID: SCR_001905
FastQC (v 0.11.3)	Babraham bioinformatics	RRID:SCR_014583
Salmon (v 0.8.2)	[55]	N/A
sleuth (v 0.28.1)	[56]	RRID:SCR_002555
clusterProfiler (v 3.8.0)	[57]	RRID:SCR_016884
MiXCR (v 2.1.10)	[58]	RRID:SCR_018725
KEGG pathway	https://www.genome.jp/kegg-bin/show_pathway?hsa04660	RRID:SCR_012773
ImmunoSEQ Analyzer Platform Adaptive Biotechnologie	Adaptive Biotechnologie	RRID:SCR_014709

RESOURCE AVAILABILITY

Lead Contact

Further information and requests for resources and reagents should be directly to and will be fulfilled by the Lead contact, Fathia Mami-Chouaib (fathia.mami-chouaib@gustaveroussy.fr)

Materials Availability

This study did not generate new unique reagents.

Data and Code Availability

The RNA sequencing dataset comparing the transcriptome of $CD8^+CD103^+$ cells with $CD8^+CD103^-$ cells, as shown in Figures 3, 4, 5, S3, and S4, Tables generated during this study are available at European Genome-phenome Archive (EGA) under EGAS00001004707 access number study.

EXPERIMENTAL MODEL AND SUBJECT DETAILS

Patient cohort characteristics and tumor samples

We conducted a monocentric retrospective study of a discovery cohort of 111 and a validation cohort of 41 advanced NSCLC patients receiving treatment with PD-1/PD-L1 inhibitors in a variety of settings covering routine clinical care, expanded access, compassionate-use programs and clinical trials (nivolumab, pembrolizumab, atezolizumab or durvalumab) at Gustave Roussy between November 2012 and February 2020. Demographic, clinical, pathological and molecular data were also collected (Tables S1 and S4). Radiological assessments were performed every 8 weeks per RECIST v1.1 and per the investigator's discretion. Fast-progressors were defined as patients who died during the first 12 weeks since the start of immunotherapy. This study was approved by the Institutional Review Board of Gustave Roussy (Commission scientifique des Essais thérapeutiques [CSET]) and informed consent was obtained. Freshly resected lung tumors and adjacent healthy lung tissue samples were obtained from the Institut mutualiste Montsouris and the Hôpital Marie-Lannelongue. For these resected tissues, the sex and the gender of the subjects are not known.

Healthy donor blood samples were collected from the French blood bank (Etablissement Français du Sang (EFS); agreement number N°12/EFS/079). The sex and the gender of the subjects are not known.

METHOD DETAILS

Immunohistochemical staining

IHC was performed on archived FFPE tumor tissues using Ventana Benchmark and Discovery automated platforms. Briefly, after deparaffinisation and epitope retrieval in CC1 buffer (pH = 8, 36 min at 95°C), tissue sections were incubated with primary mAb for ICAM-1 (clone N1C2, GeneTex, 1:200 dilution) or E-cadherin (clone EP6, Bio SB, prediluted) for 1 h at room temperature. Amplification and detection steps used the ultraview kit with amplification, and 3,3′-diaminobenzidine was used as a chromogen. ICAM-1 staining was evaluated as H-score (0 to 300) based on the percentage of tumor cells stained at each intensity (scale from 0 to 3). Since the intensity of E-cadherin staining was homogeneous within each individual tumor sample, we scored E-cadherin staining as the prominent intensity for each tumor on a semiquantitative scale from 0 to 3.

Multiplexed fluorescent IHC for CD8 T_{RM} was performed by sequential staining of a single tissue section with anti-CD8 (clone SP16, Spring Bioscience, 1:200), anti-CD103 (clone EPR4166-2, Abcam, 1:200) and anti-cytokeratin (clones AE1/AE3, Agilent, 1:100). For each staining, the HRP-conjugated amplification system was associated with a tyramide-coupled fluorophore: Opal 690, Opal 250 and Opal 570, respectively. Multispectral fluorescent images were captured using the Vectra 3 microscope (PerkinElmer) and regions of interest were selected. Image analysis using InForm software (PerkinElmer) included spectral unmixing, tissue segmentation (stromal versus epithelial areas) using a trainable classifier, nuclei detection based on dapi staining and cell segmentation followed by cell phenotyping for identification of cell populations defined by the combination of individual markers. The density (number of cells per square mm) of $CD8^+$, $CD103^+$ $CD8^+$ and $CD103^-CD8^+$ cells was determined for each tumor sample in the total tumor area, as well as in the stromal and intraepithelial compartments, based on tissue segmentation. Results from image analysis were validated for all cases.

Tumor cells and tissue-infiltrating lymphocytes isolation

Freshly resected lung tumors and adjacent healthy lung tissue samples were immediately cut into small fragments and digested for 40 min at 37°C using the tumor dissociation kit (Miltenyi Biotech). The dissociated samples were smashed on 100 μm cell strainers, washed, and red blood cell lysis was performed. CD8 T lymphocytes were positively selected using CD8 microbeads according to the manufacturer's instructions (Miltenyi Biotec). Recovered cells were either used for phenotypic analyses or further sorted by BD FACSAriaIII or BDFusion cell sorter (BD Biosciences) using anti-CD8-Pacific blue (RPA-T8, Biolegend), anti-CD103-FITC (Ber-ACT8, Biolegend) and anti-KLRG1-PE (clone 13F12F2, ebioscience) mAb. Dead cells were excluded using DAPI. $CD103^+CD8^+$ and $KLRG1^+CD8^+$ T cell populations were isolated and then either stored at −80°C for further DNA or RNA isolation or cultured for 2-5 days in the presence of low doses of IL-2 (20 U/ml) for functional studies. Tumor cells were recovered from the negative fraction of the CD8 T cell isolation described above, and then purified using a human tumor cell isolation kit (Miltenyi Biotec).

RNA and TCR sequencing and analyses

Total RNA was extracted from each sorted $CD103^+CD8^+$ and $KLRG1^+CD8^+$ TIL population pair and autologous healthy lung $CD103^+CD8^+$ lymphocytes when available; 150,000 lymphocytes per sample were processed using a single cell RNA purification kit (Norgen) according to the manufacturer's instructions. RNA integrity (RNA Integrity Score ≥ 00007.0) was checked on the Agilent 2100 Bioanalyzer and quantity was determined using Qubit (Invitrogen). The SureSelect Automated Strand-Specific RNA Library

Preparation Kit was used according to the manufacturer's instructions with the Bravo Platform. Briefly, 50 ng of total RNA sample were used for poly-A mRNA selection using oligo(dT) beads and subjected to thermal mRNA fragmentation. The fragmented mRNA samples were subjected to cDNA synthesis and were further converted into double-stranded DNA using the reagents supplied in the kit, and the resulting dsDNA was used for library preparation. The final libraries were bar-coded, purified, pooled in equal concentrations and subjected to paired-end sequencing on a HiSeq-2000 sequencer (Illumina). Fast quality was assessed using FastQC (v 0.11.3) and did not require further trimming or adaptor removal. Counting of reads over the transcriptome was performed over Gencode (v 19, GRCh37.p13) with Salmon[55] (v 0.8.2), using non-oriented library, 100 bootstrap and sequence bias correction. All other parameters were left to default. The pseudo-mapping rates were between 79% and 88% of overall reads. Differential analysis was performed within the R (v 3.2.3) environment with sleuth[56] (v 0.28.1), wasabi (v 0.1) and in-house scripts. PCA highlights inter-individual variations that are far above any variation of interest, which was confirmed by a likelihood-test ratio and taken into account within the Wald test.

Primary functional analyses were performed using Ingenuity Pathway Analysis and GSEA was performed with clusterProfiler[57] (v 3.8.0). RNaseq are available at the European Molecular Biology Laboratory European Bioinformatics Institute database (https://www.ebi.ac.uk/arrayexpress). TCR repertoire analysis was performed with a MiXCR package[58] (v 2.1.10). KEGG pathway: https://www.genome.jp/kegg-bin/show_pathway?hsa04660.

For TCRseq, total DNA from $CD103^+CD8^+$ and $KLRG1^+CD8^+$ TIL subset pairs and autologous healthy lung $CD103^+CD8^+$ cells when available, sorted from nine NSCLC patient tissues, was purified using a QIAamp DNA micro kit (QIAGEN). DNA was quantified with fluorescence-based measurement Qubit (Life Technologies). TCRβ-CDR3 sequencing was performed by ImmunoSEQ, Adaptive Biotechnologies (Seattle). Raw data of TCR reads and sequences were uploaded on the ImmunoSEQ Analyzer Platform (Adaptive Biotechnologies).

For quantitative (q) RT-PCR, total RNA was extracted from sorted cell populations using the single cell RNA purification kit (Norgen Biotek). cDNA were synthesized using the Maxima first strand cDNA synthesis kit (Thermo-Fischer Scientific). qRT-PCR was performed on a step-one plus (Applied Biosystems) using Maxima SYBR Green Master Mix (ThermoFischer Scientific). Expression levels of transcripts were normalized to 18S housekeeping gene. PCR primers for human, *TCF7, IKZF3, AHR, RORC, IL17* and *18S* genes were designed by Sigma-Aldrich and used according to the manufacturer's recommendations (Table S10).

Flow cytometry and ELISA

Phenotypic analyses were performed by direct immunofluorescence with a panel of fluorochrome-conjugated antibodies. Anti-CD3-Alexa700 (UCHT1), anti-CD8-PacificBlue (RPA-T8), anti-CD69-APC-Cy7 (FN50), anti-granzyme-B-FITC (GB11), anti-TNFα-PE/Dazzle594 (Mab11), anti-Aiolos-Alexa488 (16D9C97), anti-Vα7.2-APC-Cy7 (3C10), anti-CD161-Alexa488 (HP-3G10), anti-TCF-1-PE (7F11A10), anti-4-1BB-PE-Dazzle594 (clone 4B4-1) and anti-TCRγδ-PerCPCy5.5 (B1) were supplied by BioLegend. Anti-CD103-BV711 (Ber-ACT8), anti-IFNγ-APC (B27) and anti-Hobit-Alexa647 (Sanquin-Hobit/1) was purchased from BD Biosciences, anti-KLRG1-PE (13F12F2), anti-CD49-PerCPefluor710 (TS2/7), anti-S1PR1-APC (SW4GYPP), anti-PD-1-PeCy7 (eBioJ105), anti-AHR-PerCPefluor710 (FF3399), anti-Ki67-PerCPefluor710 (20Raj1) were supplied by Thermo Fisher Scientific. Anti-CD45RA-APC, anti-pSTAT3pS727-APC, anti-CD39-APC, anti-IL17A-PeVio770 and anti-Tbet-APC (REA102) were purchased from Miltenyi. For intracellular expression of IFNγ, TNFα and IL-17A, cells were stimulated for 4 h with PMA (50 ng/ml) plus ionomycine (1 μg/ml) in the presence of BrefeldinA (1 μg/ml, ebioscience). Cells were fixed, permeabilized (FoxP3 buffers Kit, ebioscience) and then stained with fluorochrome-conjugated mAb. Dead cells were excluded using a LIVE/DEAD Fixable UV dead cell stain kit (Thermo Fisher Scientific). Stained cells were analyzed by flow cytometry using a BD FACS Fortessa flow cytometer (BD Biosciences). Data were processed using FlowJo V10 software (Tree Star Inc.).

For ELISA, sorted $CD8^+$ T lymphocytes were stimulated overnight with PMA plus ionomycine, and then supernatants were stored until IL-17 dosage (eBiosciences).

Th17-positive control cells were generated from healthy donor's $CD4^+$ peripheral blood lymphocytes (PBL) stimulated with anti-CD3 and anti-CD28 in the presence of TGF-β and IL-6.

Conjugate formation and cytotoxic experiments

Formation of stable conjugates between T cells and autologous tumor cells was analyzed by confocal microscopy. Effector and target cells were co-cultured for 30 min at 1:1 E:T ratio, and then plated on poly-(L-lysine)-coated coverslips (Sigma-Aldrich, Saint-Louis, MO). Cells were then fixed, permeabilized as described[16] and stained with mouse anti-phospho-tyrosine (PY20, BD Biosciences) and rabbit anti-CD8 (Thermo Fisher Scientific), followed by anti-mouse AlexaFluor-488 and anti-rabbit AlexaFluor-647 (Thermo Fisher Scientific). Coverslips were mounted and analyzed using a fluorescence microscope (Leica, HR Sp8) with x63 lenses, and polarization of phospho-Tyr to the immune synapse between T cells and target cells was calculated. Stable conjugates were defined by polarization of p-Tyr at the contact zone between effector cells and tumor cells. Cytotoxic activity was evaluated using the conventional 4 h ^{51}Cr-release assay as described.[16]

QUANTIFICATION AND STATISTICAL ANALYSIS

ORR was defined as complete (CR) plus partial response (PR). OS was calculated from the date of first immunotherapy administration until death due to any cause. PFS was calculated from the date of first immunotherapy until disease progression or death due to any cause. Comparisons between patient characteristics were performed using Chi-square or Fisher's exact test for discrete variables and the unpaired t test, Wilcoxon sign-rank test or analysis of variance for continuous variables. The best cut-point for total $CD8^+$, $CD103^+$ and $CD103^-$ TIL was assessed using the log-rank maximization method.[59] Survival analyses were performed using the Kaplan-Meier method and the log-rank test. All P values inferior to 0.05 were considered statistically significant.

A Cox proportional hazards regression model was used to evaluate independent prognostic factors for OS and PFS. Variables included in the final multivariate model were selected according to their clinical relevance and statistical significance in univariate analysis (p value cut-off = 0.10). The proportional hazard hypothesis was verified with the Schoenfeld residual method. Predictive factors of disease control were tested with logistic regression in univariate and multivariate analyses. The alpha level was 5%. Statistical analyses were performed with R (free software environment for statistical computing and graphics).

Statistical significance was determined with the paired or unpaired Student t test, or with the one-way analysis of variance (ANOVA) test with Bonferroni correction. Data are presented as mean ± SEM. All statistical details of experiments can be found in Figures and Figure legends; n = number of patient or tumor/lung samples. Statistical analyses were performed with GraphPad Prism software V8 (GraphPad Software Inc., San Diego, CA). * $p < 0.05$; ** $p < 0.01$; *** $p < 0.001$ and RStudio software.

Cell Reports Medicine, Volume *1*

Supplemental Information

$CD103^+CD8^+$ T_{RM} Cells Accumulate in Tumors of Anti-PD-1-Responder Lung Cancer Patients and Are Tumor-Reactive Lymphocytes Enriched with Tc17

Stéphanie Corgnac, Ines Malenica, Laura Mezquita, Edouard Auclin, Elodie Voilin, Jamila Kacher, Heloise Halse, Laetitia Grynszpan, Nicolas Signolle, Thibault Dayris, Marine Leclerc, Nathalie Droin, Vincent de Montpréville, Olaf Mercier, Pierre Validire, Jean-Yves Scoazec, Christophe Massard, Salem Chouaib, David Planchard, Julien Adam, Benjamin Besse, and Fathia Mami-Chouaib

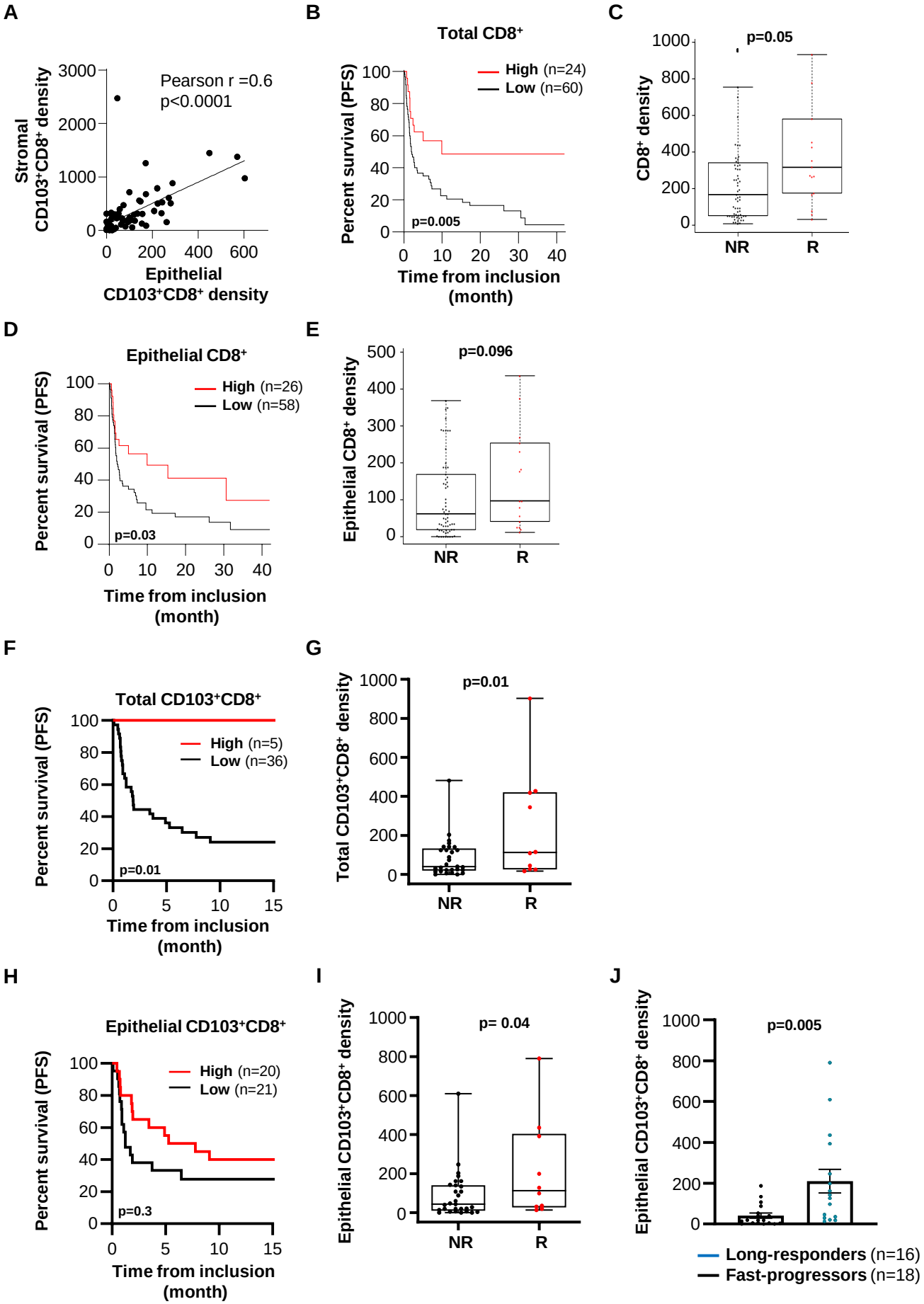
A
Stromal CD103+CD8+ density
Pearson r =0.6
p<0.0001
Epithelial CD103+CD8+ density
B
Total CD8+
High (n=24)
Low (n=60)
Percent survival (PFS)
p=0.005
Time from inclusion (month)
C
p=0.05
CD8+ density
NR
R
D
Epithelial CD8+
High (n=26)
Low (n=58)
Percent survival (PFS)
p=0.03
Time from inclusion (month)
E
p=0.096
Epithelial CD8+ density
NR
R
F
Total CD103+CD8+
High (n=5)
Low (n=36)
Percent survival (PFS)
p=0.01
Time from inclusion (month)
G
p=0.01
Total CD103+CD8+ density
NR
R
H
Epithelial CD103+CD8+
High (n=20)
Low (n=21)
Percent survival (PFS)
p=0.3
Time from inclusion (month)
I
p= 0.04
Epithelial CD103+CD8+ density
NR
R
J
p=0.005
Epithelial CD103+CD8+ density
Long-responders (n=16)
Fast-progressors (n=18)

Figure S1. Density of $CD8^+$ T cells in anti-PD-(L)1-treated patients. (Related to Figure 1)

(**A)** Correlation between the density of $CD103^+CD8^+$ cells in the stroma and in epithelial tumor regions. r-value indicates Pearson correlation coefficient. (**B)** Kaplan-Meier curve shows iPFS of PD-1 blockade-treated patients with tumors harboring a high density ($CD8^{high}$>350/mm^2) or a low density ($CD8^{low}$<350/mm^2) of $CD8^+$ cells (n=86). **(C**) Density of $CD8^+$ cells in tumors depending on iORR of non-responder (NR; n=65) and responder (R; n=17) patients to PD-1 blockade. (**D)** Kaplan-Meier curve shows iPFS of anti-PD-1-treated patients with epithelial tumor regions harboring a high (>169/mm^2) or low (<169/mm^2) density of $CD8^+$ cells (n=86). **(E)**. Density of $CD8^+$ cells in epithelial tumor regions depending on iORR of NR (n=65) and R (n=17) patients to PD-1 blockade. (**A-E)** Discovery cohort. (**F)** Kaplan-Meier curve shows iPFS of PD-1 blockade-treated patients from a validation cohort with tumors harboring high (>252/mm^2) or low (<252/mm^2) densities of $CD103^+CD8^+$ cells (n=41). **(G)** Density of total $CD103^+CD8^+$ cells in tumors depending on iORR of NR (n=29) and R (n=10) patients to PD-1 blockade. (**H)** Kaplan-Meier curve shows iPFS of anti-PD-1-treated patients with tumor epithelial regions harboring a high (>48/mm^2) or low (<48/mm^2) density of $CD103^+CD8^+$ cells. (**I)** Density of $CD103^+CD8^+$ cells in epithelial tumor regions depending on iORR of NR (n=29) and R (n=10) patients to anti-PD-1. (**J)** Density of $CD103^+CD8^+$ cells in epithelial tumor regions of anti-PD-1-treated patients undergoing a long-response (PFS>6 months and OS>12 months; n=16) or a fast-progression (defined by an "early death" occurring during the first 12 weeks since the beginning of ICB; n=18).

(F-J) validation cohort. p-value was determined by log-rank **(B**, **D, F** and **H**) or Chi2 test (**C** and **E**) or unpaired t-test (**G, I** and **J**). PFS: progression-free survival.

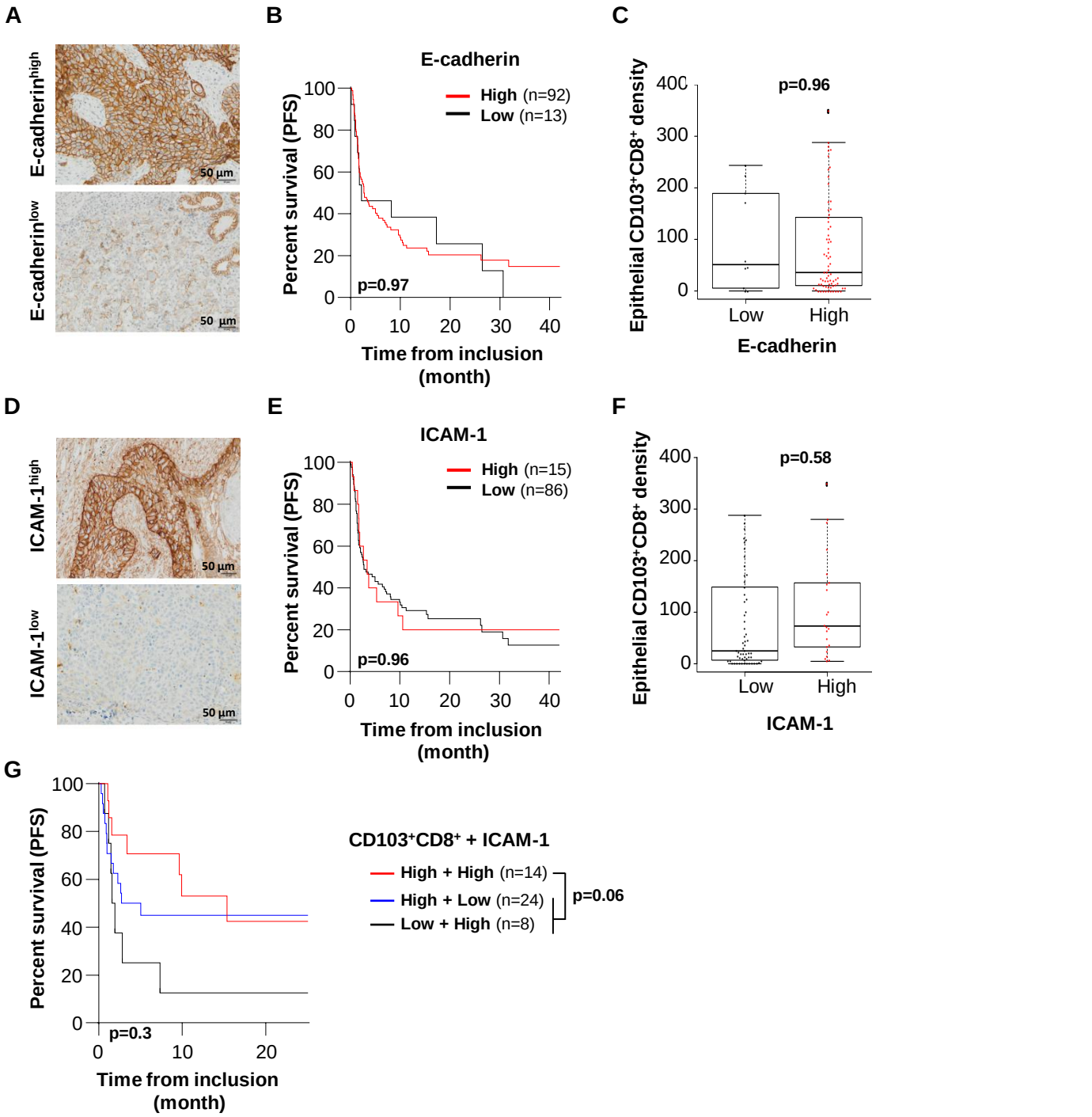

Figure S2. E-cadherin and ICAM-1 expression on tumor cells and patient survival. (Related to Figure 1)
(A) Representative images of positive and negative expression of E-cadherin by tumor cells. Scale bar 50µm (**B)** Kaplan-Meier curve shows iPFS of PD-1 blockade-treated patients with tumors harboring high and low expression of E-cadherin (n=105). **(C)** Density of $CD103^+CD8^+$ cells in epithelial tumor regions depending on E-cadherin expression on tumor cells (low, n=13; high, n=92). (**D)** Representative images of high and low expression of ICAM-1 on tumor cells. Scale bar 50µm (**E)** Kaplan-Meier curve shows iPFS of anti-PD-1-treated patients with tumors harboring high or low expression of ICAM-1 (n=101). **(F)** Density of $CD103^+CD8^+$ cells in epithelial tumor regions depending on ICAM-1 expression on tumor cells (low, n=86; high, n=15). (**G)** Kaplan-Meier curve shows iPFS of anti-PD-1-treated patients with epithelial tumor regions harboring high $CD103^+CD8^+$ infiltration and high ICAM-1 expression (red) or high $CD103^+CD8^+$ infiltration and weak expression of ICAM-1 (blue) or low $CD103^+CD8^+$ infiltration and high ICAM-1 expression (n=84). p-value was determined by log-rank test (**B, E** and **G**) or Chi2 test (**C** and **F**). The number of analyzed samples for each patient group is shown in parentheses.

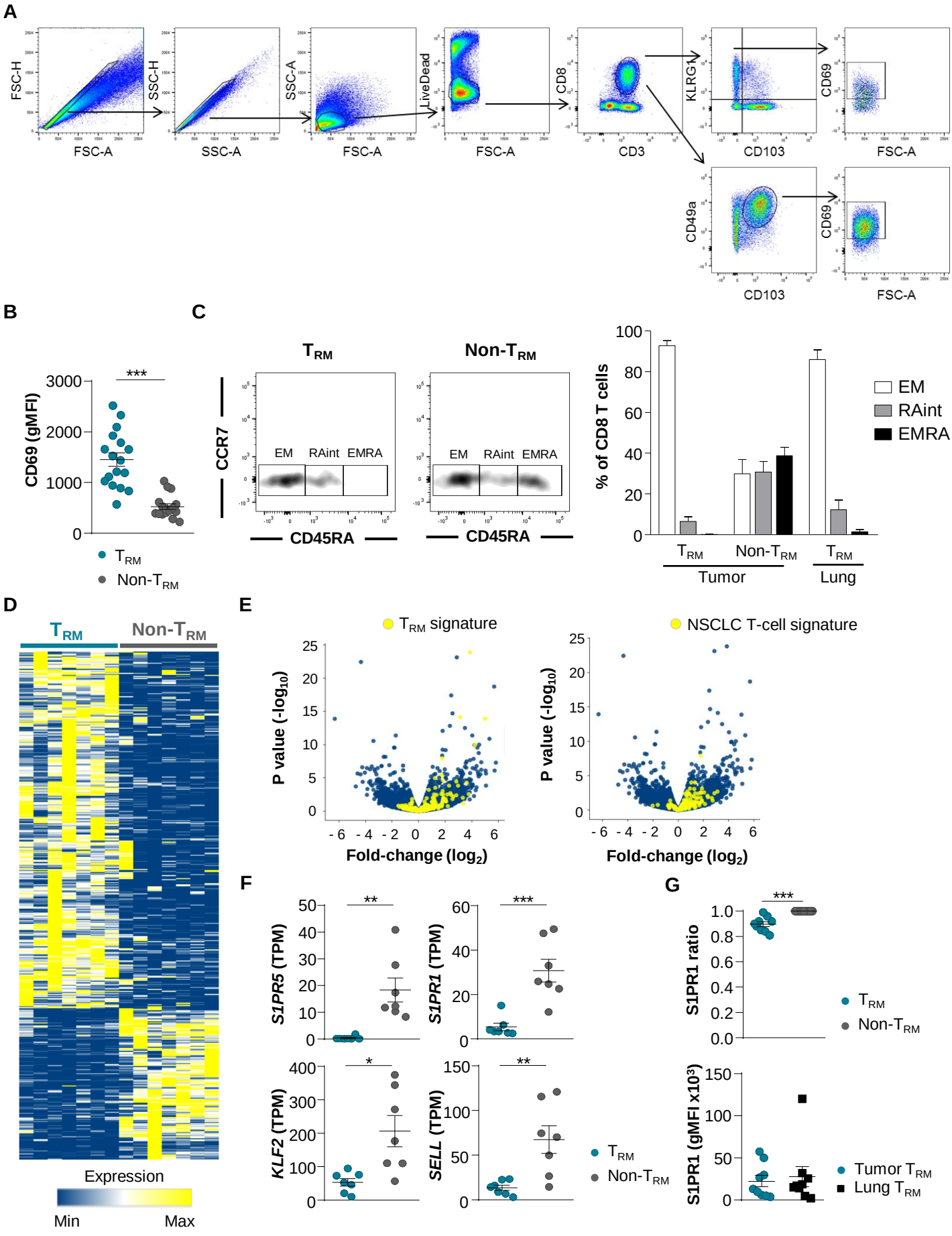
A
FSC-H
FSC-A
SSC-H
SSC-A
SSC-A
FSC-A
LiveDead
FSC-A
CD8
CD3
KLRG1
CD103
CD69
FSC-A
CD49a
CD103
CD69
FSC-A
B
CD69 (gMFI)
***
3000
2000
1000
0
TRM
Non-TRM
C
TRM
Non-TRM
CCR7
EM
RAint
EMRA
CD45RA
% of CD8 T cells
100
80
60
40
20
0
EM
RAint
EMRA
TRM
Non-TRM
TRM
Tumor
Lung
D
TRM
Non-TRM
Expression
Min
Max
E
TRM signature
NSCLC T-cell signature
P value (-log10)
Fold-change (log2)
25
20
15
10
5
0
-6 -4 -2 0 2 4 6
F
S1PR5 (TPM)
S1PR1 (TPM)
KLF2 (TPM)
SELL (TPM)
**
***
*
**
50
40
30
20
10
0
60
40
20
400
300
200
100
150
100
50
TRM
Non-TRM
G
S1PR1 ratio
***
1.0
0.8
0.6
0.4
0.2
0.0
TRM
Non-TRM
S1PR1 (gMFI x10³)
150
100
50
0
Tumor TRM
Lung TRM

Figure S3. Expression of T_{RM} markers on $CD8^+$ TIL and transcriptional profiles of $CD103^+$ (T_{RM}) and $KLRG1^+$ (non-T_{RM}) $CD8^+$ T cells. (Related to Figures 2 and 3)

(**A)** Gating strategy for analysis of KLRG1, CD103, CD49a and CD69 by $CD3^+CD8^+$ TIL. (**B)** Expression of CD69 on tumor T_{RM} and non-T_{RM} (gMFI). (**C)** Dot plot showing expression of CCR7 and CD45RA on T_{RM} and non-T_{RM} from one representative NSCLC patient. Right, percentages of effector memory (EM), effector memory CD45RA intermediate (RAint) and effector memory $CD45RA^+$ (EMRA) cells among T_{RM} and non-T_{RM} from tumor and paired T_{RM} from healthy lung (n=6). (**D)** Heat map of transcripts differentially expressed in paired $CD103^+$ and $KLRG1^+$ $CD8^+$ TIL (n=7). Genes of interest (n=500) were selected using fold-change (FC) ≥2 and p-value ≤0.05. Data were bi-clustered by transcript using Pearson's coefficient as the distance metric. The magnitude of relative expression of a particular transcript is shown in color. Each column represents an individual patient. (**E)** Differential gene expression profiles in $CD103^+$ and paired $KLRG1^+$ CD8 T cells. T_{RM} up-gene signature: all transcripts (blue), upregulated gene sets related to T_{RM} (yellow)[13]. Right, differential expression of NSCLC T-cell signature genes in tumor T_{RM} and paired non-T_{RM} (n=7). All transcripts (blue) and upregulated genes related to NSCLC T-cell signature[18] (yellow) are included. (**F)** Expression of *S1PR5, S1PR1, KLF2* and *SELL* genes in $CD103^+$ and paired $KLRG1^+$ CD8 T cells (n=7). Transcripts per million (TPM) are shown. (**G)** Ratio (T_{RM}/non-T_{RM}) of geometric mean fluorescence intensity (gMFI) of S1pr1 in paired samples of tumor T_{RM} and non-T_{RM} (n=9). Down, expression of S1pr1 (gMFI) in T_{RM} cells from tumors or paired healthy lung tissues. Histograms represent mean ± SEM. * P<0.05, ** P<0.01, *** P<0.001 (paired t-test).

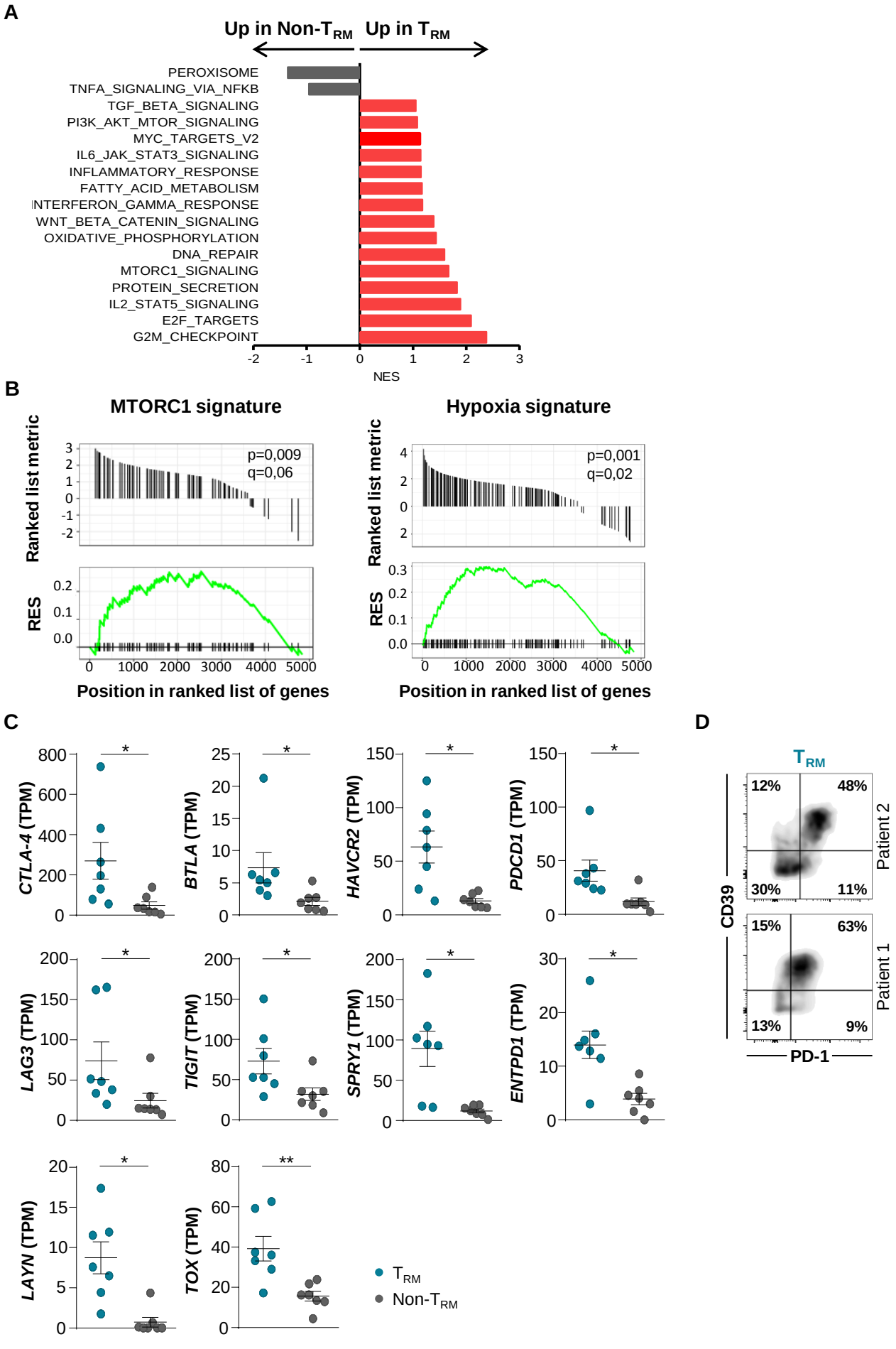
A
Up in Non-TRM
Up in TRM
PEROXISOME
TNFA_SIGNALING_VIA_NFKB
TGF_BETA_SIGNALING
PI3K_AKT_MTOR_SIGNALING
MYC_TARGETS_V2
IL6_JAK_STAT3_SIGNALING
INFLAMMATORY_RESPONSE
FATTY_ACID_METABOLISM
INTERFERON_GAMMA_RESPONSE
WNT_BETA_CATENIN_SIGNALING
OXIDATIVE_PHOSPHORYLATION
DNA_REPAIR
MTORC1_SIGNALING
PROTEIN_SECRETION
IL2_STAT5_SIGNALING
E2F_TARGETS
G2M_CHECKPOINT
-2 -1 0 1 2 3
NES
B
MTORC1 signature
Hypoxia signature
Ranked list metric
p=0,009
q=0,06
p=0,001
q=0,02
RES
Position in ranked list of genes
C
CTLA-4 (TPM)
BTLA (TPM)
HAVCR2 (TPM)
PDCD1 (TPM)
LAG3 (TPM)
TIGIT (TPM)
SPRY1 (TPM)
ENTPD1 (TPM)
LAYN (TPM)
TOX (TPM)
TRM
Non-TRM
D
TRM
CD39
PD-1
Patient 2
Patient 1
12%
48%
30%
11%
15%
63%
13%
9%

Figure S4. Transcriptional and phenotypic profiles of CD8$^+$ T_{RM} and non-T_{RM}. (Related to Figure 3)
(**A)** Gene set enrichment analysis (GSEA) of paired tumor T_{RM} and non-T_{RM} cells showing hallmark gene sets enriched in T_{RM} subset. Normalized enrichment scores (*NES*) are shown. (**B)** GSEA of mTORC1 (left) signature genes (Gene set M5924) and GSEA of hypoxia (right) signature genes (Gene set M48562) upregulated in the transcriptome of tumor T_{RM} relative to non-T_{RM}. Running enrichment score (RES) for gene set, as analysis 'walks down' ranked list of genes; position of the gene set members (black vertical lines) in ranked list of genes and value of ranking metric are shown.
(**C**) Expression of *CTLA4, BTLA, HAVCR2, PDCD1, LAG3, TIGIT, SPRY1, ENTPD1, LAYN* and *TOX* genes in CD103$^+$ and KLRG1$^+$ CD8$^+$ TIL. Values are TPM. (**D)** Representative dot plots of co-expression of CD39 and PD-1 on T_{RM} from two NSCLC patients (patients 1 and 2). Horizontal lines are mean ± SEM. * P<0.05, ** P<0.01 (paired t-test).

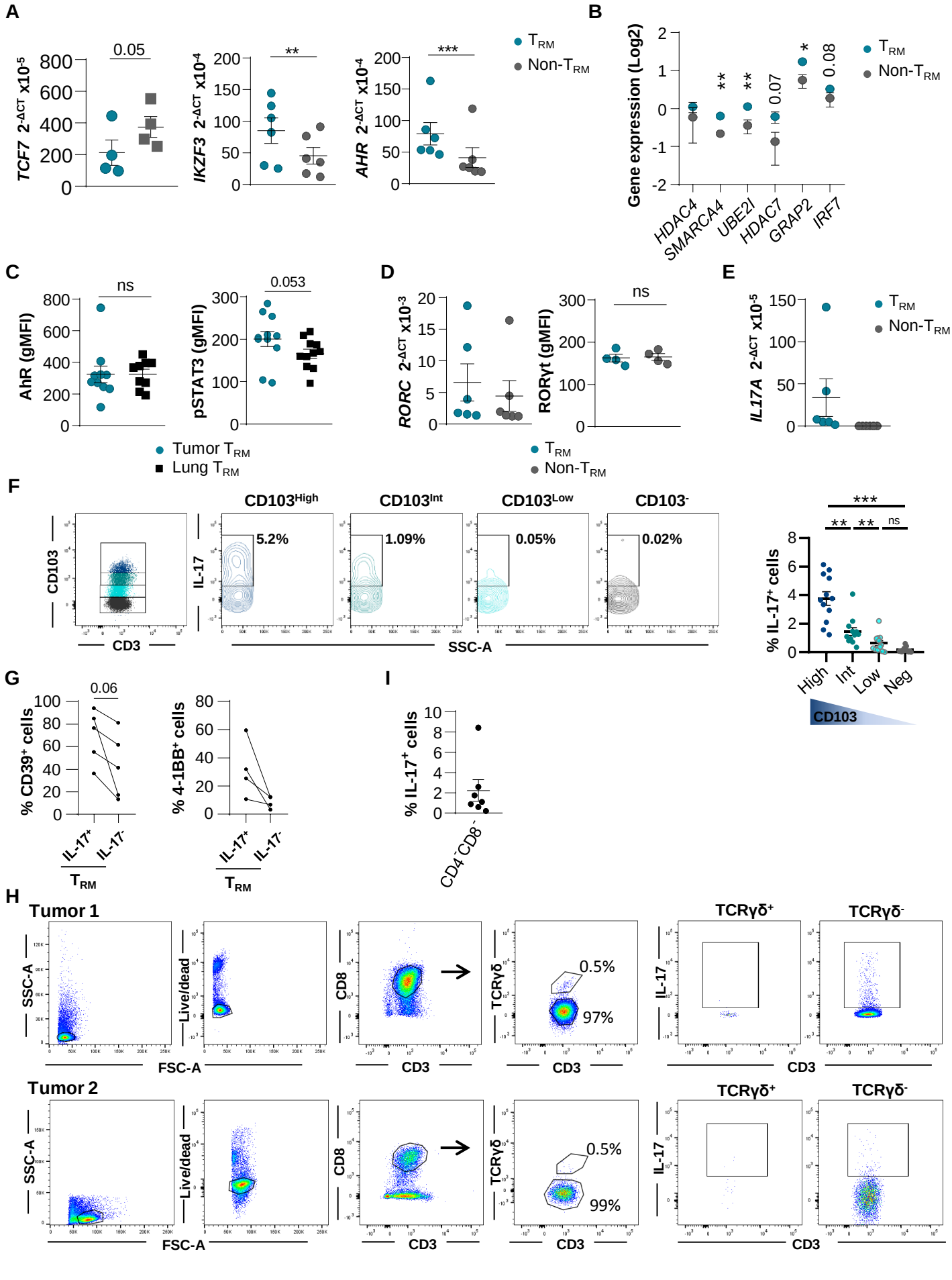
A
TCF7 2-ΔCT x10-5
0.05
IKZF3 2-ΔCT x10-4
**
AHR 2-ΔCT x10-4
***
TRM
Non-TRM
B
Gene expression (Log2)
HDAC4
SMARCA4
UBE2I
HDAC7
GRAP2
IRF7
0.07
0.08
C
AhR (gMFI)
ns
pSTAT3 (gMFI)
0.053
Tumor TRM
Lung TRM
D
RORC 2-ΔCT x10-3
RORγt (gMFI)
ns
E
IL17A 2-ΔCT x10-5
F
CD103High
CD103Int
CD103Low
CD103-
CD103
IL-17
CD3
SSC-A
5.2%
1.09%
0.05%
0.02%
% IL-17+ cells
High
Int
Low
Neg
CD103
G
% CD39+ cells
0.06
% 4-1BB+ cells
IL-17+
IL-17-
TRM
I
% IL-17+ cells
CD4-CD8-
H
Tumor 1
Tumor 2
SSC-A
FSC-A
Live/dead
CD8
CD3
TCRγδ
0.5%
97%
99%
TCRγδ+
TCRγδ-
IL-17

Figure S5. Lung tumor CD103$^+$CD8$^+$ T_{RM} display a Tc17-polarized pattern. (Related to Figures 4 and 5)
(**A)** *TCF7* (left), *IKZF3* (middle) and *AHR* (right) gene expression in T_{RM} and paired non-T_{RM} cells determined by RT-qPCR (n=4-6). Delta-CT values are shown. (**B)** Expression of genes involved in the Aiolos pathway in tumor T_{RM} and paired non-T_{RM} (n=7). Mean ± SEM of gene expression (Log2) are shown. (**C)** Expression (gMFI) of AhR (left) or pSTAT3 (right) in T_{RM} cells from tumor and paired healthy lung tissues (n=10). (**D)** Left, *RORC* gene expression (Delta-CT values) determined by RT-qPCR (n=6) and right, expression (gMFI) of RORγt in tumor T_{RM} and paired non-T_{RM} (n=4). (**E)** *IL17A* gene expression in tumor T_{RM} and paired non-T_{RM} determined by RT-qPCR (n=6). Delta-CT values are shown. (**F)** Dot plots of IL-17 expression in CD103$^+$CD8$^+$ TIL displaying CD103^{high}, CD103^{int} and CD103^{low} phenotype, and CD103$^-$CD8$^+$ TIL from one representative tumor. Right, percentages of IL-17-producing cells among CD103^{high}, CD103^{int}, CD103^{low} and CD103$^-$ TIL (n=12). **(G)** Percentages of CD39$^+$ (n=5) and 4-1BB$^+$ (n=4) cells among IL17-producing (IL-17$^+$) and IL17-non-producing (IL-17$^-$) CD103$^+$CD8$^+$ T cells from NSCLC tumors. (**H)** Dot plots of TCRγδ expression on CD3$^+$CD8$^+$ TIL from two representative tumors. Right, IL-17 production by TCRγδ$^+$ and TCRγδ$^-$ CD8$^+$ T cells stimulated 3h with PMA plus ionomycin. Two representative tumor samples are shown. (**I**). Percentages of IL-17$^+$ cells among CD8$^-$ CD4$^-$ T cells from NSCLC tumors after 4h stimulation with PMA/ionomycin (n=7). Each symbol represents one individual patient, horizontal lines are the mean ± SEM. * P<0.05 ** P<0.01, *** P<0.001 (paired t-test,**A, B, C,** and **G or** ANOVA with Bonferroni post-hoc test, **F**).

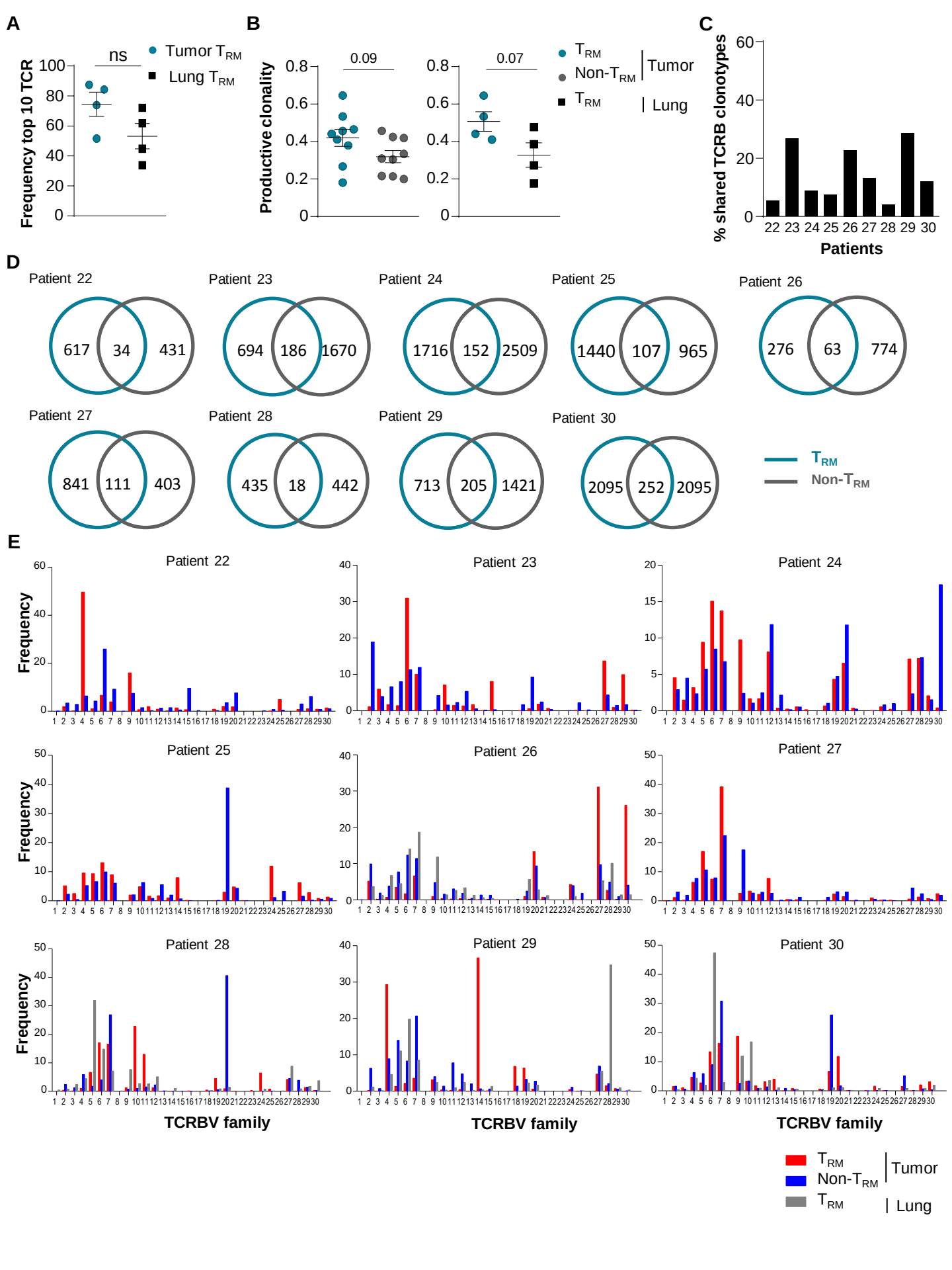
A
Frequency top 10 TCR
ns
Tumor TRM
Lung TRM
B
Productive clonality
0.09
0.07
TRM
Non-TRM
Tumor
TRM
Lung
C
% shared TCRB clonotypes
Patients
D
Patient 22
617
34
431
Patient 23
694
186
1670
Patient 24
1716
152
2509
Patient 25
1440
107
965
Patient 26
276
63
774
Patient 27
841
111
403
Patient 28
435
18
442
Patient 29
713
205
1421
Patient 30
2095
252
2095
TRM
Non-TRM
E
Patient 22
Patient 23
Patient 24
Patient 25
Patient 26
Patient 27
Patient 28
Patient 29
Patient 30
Frequency
TCRBV family
TRM
Non-TRM
Tumor
TRM
Lung

Figure S6. Tumor CD103$^+$CD8$^+$ T_{RM} displays a more oligoclonal TCR repertoire than non-T_{RM} counterparts. (Related to Figure 7)

(**A)** Frequency of the top ten TCR sequences in T_{RM} from tumors and healthy lung counterparts (n=4). (**B**) Productive clonality of tumor T_{RM} and paired non-T_{RM} (n=9). Right, productive clonality of T_{RM} from tumors and healthy lung tissues (n=4). Each symbol represents one individual patient; horizontal lines are the mean ± SEM. p-values are calculated with paired t-test. **(C)** Percentages of shared TCRβ clonotypes between tumor T_{RM} and non-T_{RM} in each patient (n=9). **(D)** Number of individual and overlap sequence diversities of TCRβ CDR3 repertoires from tumor T_{RM} and paired non-T_{RM} (n=9). (**E)** Histograms represent productive frequencies of the 30 TCRBV gene segments for tumor T_{RM} and paired non-T_{RM} (n=9), and paired healthy lung T_{RM} (n=4).

Table S1: Population description and IHC data of the discovery cohort (Related to Figure 1)

Population description		Overall population (n=86)	Density $CD103^+CD8^+$ low (n=67)	Density $CD103^+CD8^+$ high (n=19)	p-value
Age	Median, range	63 (30-84)	63 (30-84)	63 (43-73)	0.98
Gender	Female Male	27 (32%) 57 (68%)	20 (31%) 45 (69%)	7 (37%) 12 (63%)	0.62
Smoking status	Current Former Non-smoker	28 (33%) 47 (56%) 9 (11%)	22 (34%) 35 (54%) 8 (12%)	6 (32%) 12 (63%) 1 (5%)	0.75
Histology	Adenocarcinoma NSCLC, other Squamous	51 (61%) 6 (7%) 27 (32%)	41 (63%) 5(8%) 19 (29%)	10 (53%) 1 (5%) 8 (42%)	0.65
Stage at diagnosis	I-IIIA IIIB IVA- IVB NA	29 (35%) 14 (17%) 40 (48%) 0	21 (32%) 11 (17%) 33 (51%) 0	8 (44%) 3 (17%) 7 (39%) 0	0.34
Molecular status	*EGFR* mutation *ALK* fusion *KRAS mutation* *BRAF* mutation	5 (6%) 1 (1%) 19 (23%) 2 (2%)	4 (6%) 1 (2%) 14 (22%) 2 (3%)	1 (5%) 0 5 (26%) 0	0.81 0.42 0.58 0.87
Previous therapies	Platinum-based chemo Second-line chemo Other therapies No prior therapy Chemo-radiation	33 (41%) 14 (17%) 17 (21%) 6 (7%) 11 (14%)	25 (40%) 14 (11%) 17 (27%) 5 (8%) 6 (10%)	8 (44%) 4 (22%) 4 (22%) 1 (6%) 5 (28%)	0.037
Line of immunotherapy	≤ 2 > 2	45 (54%) 39 (46%)	32 (49%) 33 (51%)	13 (68%) 6 (32%)	0.14
Number of metastatic sites	≤ 2 > 2 NA	46 (55%) 38 (45%) 2	35 (54%) 30 (46%) 2	11 (58%) 8 (42%) 0	0.75
Type of immunotherapy	PD-1 inhibitor PD-L1 inhibitor	69 (82%) 15 (18%)	54 (83%) 11 (17%)	15 (79%) 4 (21%)	0.74
Performance status	0-1 ≥2 NA	68 (82%) 15 (18%) 3	50 (78%) 14 (22%) 3	18 (95%) 1 (5%) 0	0.17
Response rate	Complete response Partial response Stable disease Progressive disease NA	2 (3%) 15 (18%) 28 (34%) 37 (45%) 4	1 (2%) 8 (13%) 22 (34%) 33 (51%) 3	1 (6%) 7 (39%) 6 (33%) 4 (22%) 1	**0.024**
Objective response rate	CR + PR NA	17 (21%) 4	9 (14%) 3	8 (44%) 1	**0.005**
ICAM-1 expression	Median, range NA	80 (0-300) 3	70 (0-300) 3	140 (0-300) 0	0.23
ICAM-1 expression by category	Low High NA	61 (73%) 22 (27%) 0	49 (77%) 15 (23%) 0	12 (63%) 7 (37%) 0	0.25
E-Cadherin expression by category	0-1 2-3 NA	10 (12%) 74 (88%) 2	7 (11%) 58 (89%) 2	3 (16%) 16 (84%) 0	0.73
PD-L1 expression	Median, range NA	28 (0-100) 46	10 (0-95) 36	80 (10-100) 10	0.023
Epithelial $CD8^+$ density	Low High	59 (69%) 27 (31%)	57 (85%) 10 (15%)	2 (11%) 17 (89%)	<0.001
Density stromal $CD8^+$	Low High NA	60 (71%) 24 (29%) 2	60 (90%) 7 (10%) 0	0 17 (100%) 2	<0.001
Total $CD8^+$ density	Low High	62 (72%) 24 (28%)	61 (91%) 6 (9%)	1 (5%) 18 (95%)	<0.001
Epithelial $CD103^+CD8^+$ density	Low High	45 (52%) 41 (48%)	44 (66%) 23 (34%)	1 (5%) 18 (95%)	<0.001
Stromal $CD103^+CD8^+$ density	Low High	61 (71%) 25 (29%)	60 (90%) 7 (10%)	1 (5%) 18 (95%)	<0.001
Total $CD103^+CD8^+$ density	Low High	67 (78%) 19 (22%)	67 (100%) 0	0 19 (100%)	<0.001
Epithelial $CD103^-CD8^+$ density	Low High	41 (48%) 45 (52%)	36 (54%) 31 (46%)	5 (26%) 14 (74%)	0.01
Stromal $CD103^-CD8^+$ density	Low High	50 (58%) 36 (42%)	48 (72%) 19 (28%)	2 (11%) 17 (89%)	0.001
Total $CD103^-CD8^+$ density	Low High	70 (81%) 16 (19%)	62 (93%) 5 (7%)	8 (42%) 11 (58%)	0.001
Total $CD103^+CD8^+$ density (number)		102.59 (0;1320.75)	65.96 (0;246.8)	466.21 (252.42;1320.75)	<0.001
Epithelial $CD103^+CD8^+$ density (number)		44.56 (0;603.82)	21.56 (0;262.13)	240.23 (48.14;603.82)	<0.001
Stromal $CD103^+CD8^+$ density (number)		152.75 (0;2477.96)	93.81 (0;478.15)	678.6 (283.59;2477.96)	<0.001
Percentage of CD103+ among CD8+ in epithelial regions		76.19 (0;100)	67.48 (0;100)	83.33 (29.87;100)	0.001
Percentage of CD103+ among CD8+ in stromal regions		47.62 (0;94.44)	42.6 (0;94.44)	58.61 (26.47;87.69)	0.046

NA: not available; CR: complete response; PR: partial response.

Table S2: Immunotherapy progression-free survival (iPFS) median (Discovery cohort) (Related to Figure 1)

Variables			Total patient number	Percentage (%)	Events number	Median (95%CI) (month)	Log-rank p-value
			84	**100**	**62**	**2.69 (1.74-7.13)**	
$CD8^+$ cells	**Total**	Low	60	71.4	51	2.05 (1.51-5.03)	0.005
		High	24	28.6	11	9.92 (2.73-NR)	
	Stromal	Low	58	69	50	2.05 (1.51-5.03)	0.001
		High	24	28.6	11	30.62 (3.42-NR)	
	Epithelial	Low	58	69	48	2.22 (1.64-4.99)	0.03
		High	26	31	14	9.92 (1.74-NR)	
$CD103^+CD8^+$ cells	**Total**	Low	65	77.4	54	2.3 (1.68-5.03)	0.008
		High	19	22.6	8	30.6 (2.73-NR)	
	Stromal	Low	59	70.2	50	2.14 (1.51 -5.03)	0.006
		High	25	29.8	12	30.62 (2.30-NR)	
	Epithelial	Low	44	52.4	37	1.76 (1.48-4.99)	0.01
		High	40	47.6	25	9.63 (2.56-NR)	
$CD103^-CD8^+$ cells	**Total**	Low	68	81	55	2.5 (1.68-6.54)	0.02
		High	16	19	7	NR (1.58-NR)	
	Stromal	Low	49	58.3	43	2.14 (1.64-5.03)	0.001
		High	35	41.7	19	9.92 (1.81-NR)	
	Epithelial	Low	41	48.8	27	6.90 (2.76-26.22)	0.03
		High	43	51.2	35	1.68 (1.31-3.42)	
CD103/CD8 score	**Good**		12	14.3	5	26.22 (15.34-NR)	<0.0001
	Intermediate		57	67.9	42	2.76 (1.70-7.33)	
	Poor		15	17.9	15	1.38 (0.72-1.97)	
ICAM-1	**Low**		86	85.1	66	2.79 (1.97-7.33)	0.96
	High		15	14.9	12	3.42 (1.81-NR)	
E-cadherin	**Low**		13	12.4	11	2.23 (1.41-NR)	0.97
	High		92	87.6	73	2.74 (1.94-5.68)	
Epithelial $CD103^+CD8^+$ cells and ICAM-1	**High/High**		14	16.6	8	15.34	0.3
	High/Low		24	28.5	15	3.87	
	Low/High		8	9.5	7	1.75	

NR: not reached, CI: confidence interval

Table S3: Multivariate analysis for progression-free survival (Discovery cohort) (Related to Figure 1)

Variables	HR (95% CI)	p-value
Age ≥65	1.79 (0.73-4.37)	0.20
Histology squamous	1.5 (0.83-2.73)	0.18
Smoker	0.35 (0.14-0.84)	0.02
Performance status ≥2	1.12 (0.57-2.21)	0.73
Number of metastatic sites	1.83 (1.02-3.29)	0.04
High $CD103^{+}CD8^{+}$ density	**0.39 (0.18-0.85)**	0.02

HR: hazard ratio; CI: confidence interval.

Table S4: Population description and immunohistochemistry data of the validation cohort (Related to Figure 1)

Population description		Overall population (n=41)
Age	Median, range	64 (42-85)
Gender	Female	20 (49%)
	Male	21 (51%)
Smoking status	Current	18 (44%)
	Former	19 (46%)
	Non-smoker	4 (10%)
Histology	Adenocarcinoma	34 (83%)
	NSCLC, others	1 (2.5%)
	Squamous	6 (14.5%)
Stage at diagnosis	IIA	2 (5%)
	IIB	1 (2.5%)
	IIIA	3 (7%)
	IIIB	2 (5%)
	IVA	7 (17%)
	IVB	26 (63.5%)
Molecular status	*EGFR* mutation	2 (5%)
	ALK fusion	2 (5%)
	KRAS mutation	16 (42%)
	BRAF mutation	2 (5%)
Line of immunotherapy	≤ 2	33 (80%)
	> 2	8 (20%)
Number of metastatic sites	≤ 2	12 (29%)
	> 2	29 (71%)
Type of immunotherapy	PD-1 inhibitor	41 (100%)
Performance status	0-1	26 (63%)
	≥ 2	15 (37%)
Response rate	Complete response	2 (5%)
	Partial response	8 (20%)
	Stable disease	10 (26%)
	Progressive disease	19 (49%)
	NA	2
Objective response rate	CR + PR	10 (26%)
	NA	2
PD-L1 expression	Median, range	10 (0-100)
Epithelial $CD8^+$ density	Low	21 (51%)
	High	20 (49%)
Stromal $CD8^+$ density	Low	26 (63%)
	High	15 (37%)
Total $CD8^+$ density	Low	24 (59%)
	High	17 (41%)
Epithelial $CD103^+CD8^+$ density	Low	21 (51%)
	High	20 (49%)
Stromal $CD103^+CD8^+$ density	Low	34 (83%)
	High	7 (17%)
Total $CD103^+CD8^+$ density	Low	36 (88%)
	High	5 (12%)
Epithelial $CD103^-CD8^+$ density	Low	7 (17%)
	High	34 (83%)
Stromal $CD103^-CD8^+$ density	Low	20 (49%)
	High	21 (51%)
Total $CD103^-CD8^+$ density	Low	23 (56%)
	High	18 (44%)
Total $CD103^+CD8^+$ density (number)	Median (range)	120.4 (0;902.4)
Epithelial $CD103^+CD8^+$ density (number)	Median (range)	118 (0;789.85)
Stromal $CD103^+CD8^+$ density (number)	Median (range)	150.95 (0;1147.28)

CR: complete response; PR: partial response; NA: not available

Table S5: Patient characteristics and density of cells pre- and post-treatment (Related to Figure 1)

Group of patients	Patient N°	Number of ICB cycles	RECIST/ Radiologic response (tumor volume reduction)	Responder/ Non-responder	Stage diagnosis	OS (months)	Site of pre-biopsy	Site of post-biopsy	Days from last ICB to post-biopsy	Density of intra-epithelial $CD103^+CD8^+$ cells		Density of total $CD103^+CD8^+$ cells		Density of total $CD8^+$ cells	
										Pre-ICB	Post-ICB	Pre-ICB	Post-ICB	Pre-ICB	Post-ICB
1	**1**	7	SD	R	IIIA	11.5	Lung	Lung	24	**161**	**682**	**204**	**931**	**417**	**1779**
	2	NA	SD	R	IVB	13.9	Lung	Lung	135	**358**	**511**	**129**	**518**	**493**	**1081**
	3	NA	SD	R	IVB	14.3	Kidney meta	Kidney meta	174	162	134	173	159	729	666
	4	1	PD	NR	IVA	2	Lung	Lung	14	19	0	25	0	58	30
	5	NA	PD	NR	IIIA	18.4	Lung	Lung	34	18	6	44	21	221	600
2	**6**	1	-17%	R	NA	25.3	Lung	Lung	28	**172**	**555**	**159**	**534**	**322**	**895**
	7	1	-17%	R	IIIA	31.5	Lung	Lung	27	**25**	**155**	**33**	**155**	**135**	**342**
	8	1	-5%	NR	IB	37.1	Lung	Lung	21	230	133	258	322	1691	1775
	9	1	0%	NR	IIA	31.2	Lung	Lung	25	267	95	208	225	781	538

ICB: immune checkpoint blockade, OS : overall survival ; SD: stable disease; PD: progressive disease; R: responder; NR: non-responder; Meta: metastasis; NA: not available

Table S6: Population description of ICAM and E-cadherin cohort (Discovery cohort) (Related to Figure 1)

Population description		Overall population (N=111)
Age	Median, range	63 (30-92)
Gender	Female	35 (32%)
	Male	76 (68%)
Smoking status	Current	36 (32%)
	Former	64 (58%)
	Non-smoker	11 (10%)
Histology	Adenocarcinoma	66 (60%)
	NSCLC, other	16 (14%)
	Squamous	29 (26%)
Stage at diagnosis	I-IIIA	4 (4%)
	IIIB	11 (10%)
	IVA- IVB	95 (86%)
	Missing	1
Molecular status	*EGFR* mutation	5 (6%)
	ALK fusion	2 (2%)
	KRAS mutation	24 (30%)
	BRAF mutation	3 (4%)
Previous therapies	Platinum-based chemo	55 (50%)
	Second-line chemo	14 (13%)
	Other therapies	22 (20%)
	No prior therapy	6 (5%)
	Chemo-radiation	13 (12%)
Line of immunotherapy	≤ 2	64 (58%)
	> 2	47 (42%)
Number of metastatic sites	≤ 2	54 (49%)
	> 2	57 (51%)
	Missing	0
Type of immunotherapy	PD-1 inhibitor	96 (86%)
	PD-L1 inhibitor	15 (14%)
Performance status	0-1	90 (82%)
	≥2	20 (18%)
	Missing	1
Response rate	Complete response	2 (2%)
	Partial response	23 (22%)
	Stable disease	38 (36%)
	Progressive disease	44 (40%)
	Missing	4
Objective response rate	CR + PR	63 (58%)
	Missing	3
ICAM-1 expression	Median range	80 (0-300)
	Missing	10
ICAM-1 expression by category	Low	86 (85%)
	High	15 (15%)
	Missing	10
E-Cadherin expression by category	0-1	13 (12%)
	2-3	92 (88%)
	Missing	6

CR: complete response; PR: partial response.

Table S7: Frequencies of T_{RM} and non-T_{RM} cells in lung tumors and autologous adjacent normal lung tissues (Related to Figure 2)

	Lung tumor				Adjacent normal lung			
Patient	**$CD103^+CD49a^+CD49a^+$**		**$KLRG1^+$**		**$CD103^+CD49a^+CD49a^+$**		**$KLRG1^+$**	
	%	**Number/mg**	**%**	**Number/mg**	**%**	**Number/mg**	**%**	**Number/mg**
1	55	320	28	164	56	44	28	22
2	52	2340	31	1271	31	44	38	47
3	44	614	37	515	8	76	85	845
4	27	354	53	706	25	369	44	656
5	36	57	41	67	7	48	57	394
6	37	374	40	401	28	12	46	20
7	62	781	20	254	13	315	77	1881
8	30	3013	37	3767	27	64	61	144
9	25	143	50	287	5	6	79	111
10	81	540	10	70	41	49	30	36
11	35	314	32	310	43	126	31	90
12	87	3823	5	204	52	44	24	22
13	51	547	23	249	2	17	82	623
14	80	1727	4	93	59	640	6	60
15	48	368	31	238	16	28	51	89
16	59	797	15	204	28	85	21	63
17	40	133	38	126	2	1	91	37
18	67	499	18	135	49	81	13	22

The total number of T_{RM} per milligram of tissue was included

Table S8: Differential gene expression profiles of CD103$^+$CD8$^+$ TIL and autologous KLRG1$^+$CD8$^+$ TIL (Related to Figures 3, 4 and 5)

Gene	Fold change	p-value
Activation/Th17		
IL17A	23.62	$1.08\ 10^{-10}$
TNFSF4	20.32	$1.69\ 10^{-7}$
TMIGD2	9.32	$8.97\ 10^{-4}$
IL12RB2	7.87	$5.28\ 10^{-4}$
CKLF	7.74	$3.74\ 10^{-3}$
CD2	7.32	$3.67\ 10^{-3}$
CD82	7.26	$6.52\ 10^{-3}$
CPNE1	7.25	$5.64\ 10^{-3}$
ICOS	6.72	$4.59\ 10^{-3}$
CD6	6.61	$4.29\ 10^{-2}$
CD226	6.12	$1.33\ 10^{-3}$
IL26	5.69	$1.41\ 10^{-4}$
CD63	5.53	$8.10\ 10^{-3}$
CD109	5.21	$2.61\ 10^{-2}$
IL32	5.11	$2.81\ 10^{-2}$
CSF2	4.36	$3.76\ 10^{-3}$
IRF5	4.31	$1.02\ 10^{-2}$
CD101	4.08	$9.70\ 10^{-9}$
CD70	3.21	$1.14\ 10^{-2}$
CD7	2.99	$3.76\ 10^{-2}$
RABGEF1	2.99	$3.80\ 10^{-2}$
HAVCR1	2.90	$1.26\ 10^{-2}$
IL17RA	2.75	$2.88\ 10^{-2}$
GZMB	2.54	$5.54\ 10^{-4}$
IL18RAP	2.20	$7.86\ 10^{-3}$
IFNG	1.99	$4.44\ 10^{-2}$
GZMA	1.68	$2.89\ 10^{-2}$
CD244	1.52	$1.18\ 10^{-2}$
IL2RG	1.45	$4.89\ 10^{-2}$
TNFRSF25	1.39	$2.34\ 10^{-2}$
TGFBR3	-1.64	$1.81\ 10^{-2}$
IL15	-1.96	$3.90\ 10^{-2}$
CD28	-2.13	$3.97\ 10^{-3}$
GZMK	-3.44	$7.07\ 10^{-3}$
IL12A	-3.47	$7.91\ 10^{-3}$
Inhibition/exhaustion		
ENTPD1	56.05	$5.21\ 10^{-9}$
LAYN	21.84	$1.22\ 10^{-9}$
SPRY1	9.09	$2.28\ 10^{-4}$
CD200	7.74	$2.71\ 10^{-3}$
CTLA4	5.14	$1.48\ 10^{-2}$
BTLA	4.70	$1.98\ 10^{-3}$
HAVCR2	2.78	$3.66\ 10^{-3}$
PDCD1	2.63	$1.79\ 10^{-2}$
LAG3	2.20	$8.93\ 10^{-3}$
TIGIT	1.86	$5.22\ 10^{-3}$
CBLB	1.43	$4.85\ 10^{-2}$
TOX	1.96	$3.15\ 10^{-4}$
TOX2	12.96	$3.71\ 10^{-4}$
SPRY2	-2.91	$3.97\ 10^{-2}$
Transcription factors		
IKZF3	17.93	$6.01\ 10^{-3}$
ATP8B4	17.50	$1.53\ 10^{-8}$
GFI1	9.24	$5.20\ 10^{-4}$
IRF3	7.75	$9.65\ 10^{-4}$
ZEB1	7.38	$8.53\ 10^{-4}$
ZNF683	6.55	$4.10\ 10^{-4}$
ZNF384	5.28	$3.91\ 10^{-2}$
FOXJ3	5.22	$1.72\ 10^{-2}$
IKZF4	5.05	$1.10\ 10^{-2}$
FOXP3	4.80	$9.39\ 10^{-4}$
BACH1	4.43	$1.62\ 10^{-2}$
E2F7	4.00	$5.09\ 10^{-2}$
ATF2	3.90	$2.29\ 10^{-2}$
ZBED2	3.89	$5.34\ 10^{-7}$
PRDM1	3.87	$7.71\ 10^{-3}$
TSC2	3.77	$2.20\ 10^{-2}$
PRDM5	3.53	$1.08\ 10^{-2}$
IKBKB	3.40	$2.84\ 10^{-2}$
BATF3	3.03	$2.86\ 10^{-2}$
PRDM2	2.72	$4.35\ 10^{-2}$
RUNX2	2.50	$3.70\ 10^{-2}$
RUNX3	2.24	$1.95\ 10^{-3}$
E2F2	2.13	$2.45\ 10^{-2}$
IKZF3	2.01	$1.54\ 10^{-3}$
BATF	1.52	$4.20\ 10^{-2}$
E2F3	-1.60	$2.35\ 10^{-2}$
IKZF2	-1.63	$2.06\ 10^{-2}$
BCL6	-1.93	$2.13\ 10^{-2}$
EOMES	-2.38	$1.34\ 10^{-3}$
KLF2	-2.58	$8.57\ 10^{-4}$
KLF3	-3.60	$1.26\ 10^{-3}$
TCF7	-4.03	$1.39\ 10^{-2}$
Adhesion/migration		
ITGAE	31.99	$1.37\ 10^{-14}$
CXCL13	18.40	$1.28\ 10^{-10}$
ITGA7	8.16	$2.30\ 10^{-3}$
KLRC1	8.10	$1.81\ 10^{-4}$
CCR5	6.41	$1.90\ 10^{-2}$
ITGA1	5.96	$6.27\ 10^{-3}$
VCAM1	5.27	$1.59\ 10^{-2}$
CD9	5.25	$1.32\ 10^{-2}$
IIK	4.63	$5.04\ 10^{-2}$
ITGB7	4.17	$3.69\ 10^{-2}$
CCR6	3.86	$4.03\ 10^{-2}$
CXCR6	3.54	$3.28\ 10^{-3}$
ITGAD	3.47	$1.69\ 10^{-3}$
CD248	2.64	$1.61\ 10^{-2}$
KIRC2	2.54	$4.00\ 10^{-2}$
CD44	-1.61	$2.73\ 10^{-2}$
CXCR5	-1.89	$1.31\ 10^{-2}$
CCR4	-2.29	$1.93\ 10^{-2}$
CCR7	-2.68	$1.34\ 10^{-3}$
ITGA5	-3.62	$1.36\ 10^{-2}$
ITGAM	-3.67	$4.45\ 10^{-2}$
SELL	-4.88	$1.12\ 10^{-2}$
S1PR1	-5.12	$3.80\ 10^{-2}$
KIRF1	-5.23	$1.58\ 10^{-3}$
CXCR2	-8.84	$2.02\ 10^{-3}$
CXCR1	-8.99	$3.23\ 10^{-9}$
CX3CR1	-10.57	$2.67\ 10^{-11}$
KLRG1	-14.79	$3.38\ 10^{-7}$
ICAM2	-19.03	$2.51\ 10^{-7}$
S1PR5	-20.95	$3.07\ 10^{-9}$
T_{RM} signature		
GSG2	8.75	$4.73\ 10^{-20}$
GPR34	7.45	$8.42\ 10^{-7}$
ITGAE	5.90	$1.51\ 10^{-28}$
CXCR6	3.29	$3.89\ 10^{-9}$
ACP5	2.64	$5.14\ 10^{-7}$
LDLRAD4	2.33	$1.28\ 10^{-7}$
AMICA1	2.21	$9.58\ 10^{-7}$
ATP10D	2.15	$2.28\ 10^{-7}$
IFNG	2.00	$3.24\ 10^{-3}$
ABTB2	1.83	$1.24\ 10^{-2}$
QPCT	1.80	$6.25\ 10^{-2}$
XCL1	1.67	$2.53\ 10^{-2}$
CD244	1.59	$4.16\ 10^{-7}$
KCNN4	1.57	$2.78\ 10^{-2}$
RACGAP1	1.53	$8.43\ 10^{-2}$
MAPKAPK3	1.52	$6.95\ 10^{-4}$
P2RY10	1.45	$6.20\ 10^{-2}$
CCL5	1.42	$5.59\ 10^{-2}$
PCED1B	1.41	$1.04\ 10^{-2}$
VOPP1	1.31	$2.05\ 10^{-2}$
ABI3	1.30	$3.85\ 10^{-2}$
DOCK2	1.27	$5.22\ 10^{-2}$
CDC25B	-1.22	$6.84\ 10^{-2}$
LITAF	-1.25	$3.67\ 10^{-2}$
NEDD4	-1.36	$4.25\ 10^{-2}$
BCL9L	-1.38	$2.85\ 10^{-2}$
STK38	-1.41	$1.52\ 10^{-3}$
FAM65B	-1.48	$6.78\ 10^{-2}$
SAMHD1	-1.50	$1.78\ 10^{-7}$
FRMD4B	-1.84	$2.72\ 10^{-2}$
LEF1	-1.87	$8.56\ 10^{-7}$
PDE2A	-1.90	$9.30\ 10^{-2}$
ICAM2	-1.94	$2.59\ 10^{-4}$
RASA3	-2.34	$1.88\ 10^{-7}$
EOMES	-2.35	$2.18\ 10^{-7}$
KLF2	-2.46	$1.58\ 10^{-4}$
TCF7	-2.47	$7.30\ 10^{-4}$
FAM49A	-2.95	$9.02\ 10^{-7}$
KLF3	-3.57	$3.29\ 10^{-9}$
S1PR1	-3.62	$5.05\ 10^{-10}$
S1PR5	-19.54	$3.11\ 10^{-10}$
Lung cancer T-cell signature		
CTLA4	3.45	$3.63\ 10^{-4}$
CXCR6	3.29	$3.89\ 10^{-9}$
PDCD1	2.43	$5.61\ 10^{-9}$
SIRPG	2.43	$8.78\ 10^{-4}$
PTPN22	1.98	$2.52\ 10^{-7}$
CD2	1.85	$7.75\ 10^{-4}$
SIT1	1.70	$2.32\ 10^{-3}$
TIGIT	1.71	$1.41\ 10^{-2}$
UBASH3A	1.60	$4.88\ 10^{-3}$
GPR174	1.59	$6.17\ 10^{-3}$
CD96	1.56	$1.82\ 10^{-2}$
SLAMF1	1.51	$6.32\ 10^{-2}$
SLA2	1.49	$8.64\ 10^{-3}$
CCR5	1.45	$5.51\ 10^{-2}$
P2RY10	1.45	$6.20\ 10^{-2}$
CCL5	1.42	$5.59\ 10^{-2}$
LCK	1.41	$2.99\ 10^{-2}$
SASH3	1.37	$7.11\ 10^{-2}$
TBC1D10C	1.37	$9.11\ 10^{-2}$
IL2RG	1.33	$2.67\ 10^{-2}$
IL12RB1	1.25	$7.00\ 10^{-2}$
CST7	-1.54	$2.73\ 10^{-2}$

Table S9: **Hallmark gene sets enriched in T_{RM} cells (Related to Figure 4)**

Hallmark gene set	NES	p-value	Core enrichment
TNFA_SIGNALING_VIA_NFKB	-0,95	0,54	ZBTB10,SQSTM1,CLCF1,DENND5A,KLF2,CFLAR,IFNGR2,ICAM1,ACKR3,PLEK,NINJ1,SOD2,SLC2A6
PEROXISOME	-1,35	0,11	LONP2,SOD2,IDE,TSPO,SLC23A2
TGF_BETA_SIGNALING	1,05	0,42	NCOR2,SMURF2,CTNNB1
PI3K_AKT_MTOR_SIGNALING	1,08	0,39	CAMK4,PIK3R3,TSC2,MKNK1,RPS6KA1,CDK1,MYD88,AP2M1,MAPKAP1,CDK1,ACTR2,FASLG,ARPC3,MKNK1,RAF1,RPS6KA3,PIN1,CAB39,RPTOR
MYC_TARGETS_V2	1,13	0,32	LAS1L,UNG,PES1,MCM5,TBRG4,SLC19A1,PLK4,MCM4,MCM5,IMP4
IL6_JAK_STAT3_SIGNALING	1,14	0,29	CXCL13,CD9,IL4R,CSF2,MYD88,CSF1,IRF9,CSF1,IL17RA,ITGA4,EBI3,FAS,IL6ST,
INFLAMMATORY_RESPONSE	1,15	0,27	ABI1,CD82,SRI,P2RX4,SRI,P2RX7,NLRP3,IRF7,ATP2C1,IL4R,LTA,SEMA4D
FATTY_ACID_METABOLISM	1,17	0,28	DLST,GCDH,ECI2,PPARA,ACOX1,AUH,ECI2,SDHC,CRYZ,HPGD,D2HGDH,GSTZ1,HIBCH,ECI2
INTERFERON_GAMMA_RESPONSE	1,18	0,25	PTPN6,DDX58,SRI,TRIM25,VCAM1,IRF7,IL4R,NCOA3,GPR18,RNF31,IRF5,TRAFD1,RNF31,ITGB7,MYD88,ST3GAL5,RSAD2,IFI35,IFNAR2,XAF1,IRF9
WNT_BETA_CATENIN_SIGNALING	1,39	0,11	NCOR2,RBPJ,PPARD,CTNNB1,NCSTN,JAG2,NCSTN,NUMB
OXIDATIVE_PHOSPHORYLATION	1,43	0,07	SLC25A12,ATP6V1H,DLST,COX4I1,NDUFV1,BAX,IMMT,MGST3,VDAC3,NNT,MAOB,ATP5A1,PHYH,SLC25A11,ATP6V0B,RHOT1,SDHC,ATP5G1,ATP5G2, HTRA2,MGST3,ATP5J,ATP5L
DNA_REPAIR	1,59	0,02	RNMT,NME3,LIG1,TAF6,NT5C,ERCC2,POLA2,ZWINT,TSG101,RAD51,ERCC2,ZWINT,POLD1,ITPA,PRIM1,POLD3,POLR1C,CANT1,POLR2D,GTF2H3
MTORC_SIGNALING	1,67	0,01	BUB1,QDPR,AURKA,SYTL2,SYTL2,CDC25A,PIK3R3,ELOVL6,SHMT2,GSR,CD9,VLDLR,IMMT,DHFR,UNG,RRM2,SYTL2,ASNS,AURKA,UCHL5,EPRS,CCT6A,TFRC,AK4,SYTL2,PFKL,ATP5G1,PSMA4,SYTL2,TFRC,EBP,TM7SF2,NFYC,ACTR2,P4HA1,NAMPT,MTHFD2,FDXR,MCM4,G6PD,GBE1,SYTL2,MCM4,STIP1,NAMPT,HMBS,SYTL2
PROTEIN_SECRETION	1,83	0,01	STX16,ATP6V1H,SEC31A,CD63,TSG101,PAM,ARFIP1,VPS45,RAB2A,PAM,AP2M1,GOLGA4,COPB1,ICA1,SGMS1,CLTA,GOSR2,SGMS1,SNAP23,TPD52
IL2_STAT5_SIGNALING	1,89	0,001	ITGAE,CAPG,NCS1,BCL2L1,HOPX,ICOS,TNFRSF8,MYO1E,P2RX4,SNX14,CTLA4,IKZF4,RABGAP1L,IL4R,NCOA3,FLT3LG,FAH,PHTF2,MYO1E,CSF2,TNFRSF8, ST3GAL4,PLAGL1,PLEC,MYO1C
E2F_TARGETS	2,09	0,001	ILF3,BUB1B,MELK,LIG1,BIRC5,DLGAP5,AURKA,CDC25A,CIT,POLA2,ESPL1,MELK,WDR90,AURKB,MCM3,RAD51C,BRCA1,HMMR,SMC4,POLD1,UNG,POLD2,RRM2,CDK1,POLD3,STAG1,MKI67,RAD51AP1,PSMC3IP,AURKA,CDKN2A,SMC4,BRCA2,CDKN3,WEE1,CENPE,AURKB,GINS3,TFRC,EIF2S1,NUP107,MYBL2,AURKB,TMPO,RACGAP1,MCM5,TBRG4,CENPM,KIF2C,TFRC,CDC20,LIG1,ORC6,CDK1,ATAD2,CCNE1,CDCA3,EZH2,RFC2,DEPDC1,SMC4,SPAG5,CIT,CDCA3,HELLS,SMC4,STAG1,MTHFD2,RAD51AP1,POLE,TCF19,CKS1B,PRKDC,PLK4,MCM4,DNMT1,SMC6,CDKN2A,TRIP13,POLD3,DEK,EXOSC8,PLK4,KPNA2,RAD51C,BARD1
G2M_CHECKPOINT	2,38	0,001	ILF3,MTF2,SMC2,BUB1,PRC1,BIRC5,TPX2,AURKA,CDC25A,NUSAP1,KIF15,EXO1,TROAP,POLA2,ESPL1,NUSAP1,AURKB,MCM3,KIF23,HMMR,PRC1,SMC4,SMC2,CBX1,TLE3,STIL,TNPO2,CDK1,STAG1,CHMP1A,MKI67,KIF23,AURKA,NUSAP1,TRAIP,BRCA2,EXO1,TTK,SS18,SS18,CDKN3,ODF2,CENPE,CDC7,AURKB,DKC1,CASP8AP2,PBK,CDC27,TROAP,MYBL2,AURKB,EWSR1,TRAIP,KIF23,TMPO,RACGAP1,MCM5,SMC2,TRAIP,KIF2C,SRSF10,CDC20, ORC6,PAFAH1B1,CDK1,RBM14,EZH2

NES: Normalized enrichment score

Table S10: Primer pair sequences for RT-PCR (Related to STAR methods)

IKZF3 Forward	AGATTTGAATGTGCCCTGGT
IKZF3 Reverse	TGTCTTGCCTCCGCACTT
RORC Forward	CTTGCCGTAGGGATGTCTCG
RORC Reverse	GAAGTTCCGTCAGCCCGTT
AHR Forward	TAACCCAGACCAGATTCCTCCAGA
AHR Reverse	CCCTTGGAAATTCATTGCCAGA
IL17A Forward	AACGATGACTCCTGGGAAGA
IL17A Reverse	GGATTTCGTGGGATTGTGAT
TCF7 Forward	CGGGACAGGACCATTACAACTAGATCAAGGAC
TCF7 Reverse	CCACCTGCCTCGGCCTGCCAAAGT
S1PR1 Forward	CAGACAAGCAAAACAAAGTG
S1PR1 Reverse	CATCAACAAAAGTGCCAAAG
18S Forward	CGGACAGGATTGACAGATTG
18S Reverse	CAATCGCTCCACCAACTAA